# Improved detection of abrupt change in vegetation reveals dominant fractional woody cover decline in Eastern Africa

Abera, Temesgen

2022-03-15

Abera , T , Heiskanen , J , Maeda , E , Hailu , B T & Pellikka , P 2022 , ' Improved detection of abrupt change in vegetation reveals dominant fractional woody cover decline in Eastern Africa ' , Remote Sensing of Environment , vol. 271 , no. 112897 , 112897 . https://doi.org/10.1016/j.rse.2022.112897

http://hdl.handle.net/10138/339652
https://doi.org/10.1016/j.rse.2022.112897

Remote Sensing of Environment 271 (2022) 112897

Contents lists available at ScienceDirect

Remote Sensing of Environment

journal homepage: www.elsevier.com/locate/rse

# Improved detection of abrupt change in vegetation reveals dominant fractional woody cover decline in Eastern Africa

Temesgen Alemayehu Abera [a,b,*], Janne Heiskanen [a,b], Eduardo Eiji Maeda [a,e], Binyam Tesfaw Hailu [a,c], Petri K.E. Pellikka [a,b,d]

[a] Department of Geosciences and Geography, P.O. Box 68, FI-00014, University of Helsinki, Finland
[b] Institute for Atmospheric and Earth System Research, Faculty of Science, University of Helsinki, Finland
[c] School of Earth Sciences, Addis Ababa University, P.O.Box 1176, Addis Ababa, Ethiopia
[d] State Key Laboratory for Information Engineering in Surveying, Mapping and Remote Sensing, Wuhan University, Wuhan 430079, China
[e] Division of Ecology and Biodiversity, Faculty of Science, The University of Hong Kong, Hong Kong, China

ARTICLE INFO

Editor: Marie Weiss

*Keywords:*
Woody cover change
Abrupt change
Gradual change
Airborne laser scanning (ALS)
Machine learning
Breakpoint detection

ABSTRACT

While cropland expansion and demand for woodfuel exert increasing pressure on woody vegetation in East Africa, climate change is inducing woody cover gain. It is however unclear if these contrasting patterns have led to net fractional woody cover loss or gain. Here we used non-parametric fractional woody cover (WC) predictions and breakpoint detection algorithms driven by satellite observations (Landsat and MODIS) and airborne laser scanning to unveil the net fractional WC change during 2001–2019 over Ethiopia and Kenya. Our results show that total WC loss was 4-times higher than total gain, leading to net loss. The contribution of abrupt WC loss (59%) was higher than gradual losses (41%). We estimated an annual WC loss rate of up to 5% locally, with cropland expansion contributing to 57% of the total loss in the region. Major hotspots of WC loss and degradation corridors were identified inside as well as surrounding protected areas, in agricultural lands located close to agropastoral and pastoral livelihood zones, and near highly populated areas. As the dominant vegetation type in the region, Acacia-Commiphora bushlands and thickets ecosystem was the most threatened, accounting 69% of the total WC loss, followed by montane forest (12%). Although highly outweighed by loss, relatively more gain was observed in woody savanna than in other ecosystems. These results reveal the marked impact of human activities on woody vegetation and highlight the importance of protecting endangered ecosystems from increased human activities for mitigating impacts on climate and supporting sustainable ecosystem service provision in East Africa.

## 1. Introduction

Woody vegetation cover in Africa is highly dynamic. Loss from deforestation and gain from enhanced atmospheric CO2 concentration, changing rainfall patterns, and other local factors (e.g., change in fire frequency and herbivore densities) are inducing contrasting woody cover change patterns, having a direct impact on terrestrial energy fluxes (Forzieri et al., 2020), carbon stock and global CO2 variability (Brandt et al., 2017; Venter et al., 2018; Williams et al., 2007). With the United Nation Decade on Ecosystem Restoration (2021−2030) demanding every continent to prevent, halt and reverse the degradation of ecosystems, Africa is aiming to take the challenges of restoring 100 million hectares of land by 2030 under the African Forest Landscape Restoration Initiative (AFR100). For successful implementation of such initiative as well as sustaining ecosystem service provision in the region, understanding woody cover dynamics is crucial.

Particularly in East Africa (EA), changes in woody cover (WC) are highly prevalent. While woodfuels (charcoal and firewood) are the primary sources of household energy supply, accounting for more than 70% of the energy source (Sola et al., 2017; UNEP, 2016), their production directly affects the extent and quality of WC through deforestation and forest degradation (Chidumayo and Gumbo, 2013). Similarly, agriculture being the major contributor to the economy (Rippke et al., 2016), cropland expansion often occurs at the cost of woody vegetation (Brink et al., 2014). With projected population expected to double by 2050, demand for more crop production and woodfuel poses increasing

* Corresponding author at: Department of Geosciences and Geography, P.O. Box 68, FI-00014, University of Helsinki, Finland.
*E-mail address:* temesgen.abera@helsinki.fi (T.A. Abera).

https://doi.org/10.1016/j.rse.2022.112897
Received 11 May 2021; Received in revised form 22 November 2021; Accepted 4 January 2022
Available online 10 January 2022

pressure on the already threatened woody vegetation in this region (Stévart et al., 2019).

Conservation of wildlife is increasingly important for maintaining biodiversity; but it has also found to locally cause decrease of woody cover and above ground carbon stocks (Amara et al., 2020) especially in savannah landscape where high wildlife (browsers) density put pressure on woody cover. Together with agricultural expansion and rising fuelwood demand, there is a trend of decreasing above ground biomass and carbon sequestration in the lowlands of East Africa while in highlands there is evidence of increase in woody cover at places (Pellikka et al., 2018). For mitigating these risks, reversing ecosystem degradation, and achieving environmental sustainability, improving WC monitoring capabilities is important.

Satellite observation data provide a viable option to monitor WC. With high spatial resolution, temporal frequency, and multiple spectral information, satellite observations support WC monitoring from local to global scale efficiently. In this regard, Landsat (with 30 m spatial resolution, 40+ years of data record since its first launch in 1972, and 16-day temporal frequency), MODIS (250 m, 500 m, and 1000 m resolution, 20+ years of data collection since its launch in 1999, and daily temporal frequency), Sentinel 1, 2 (6+ years data record since operational in 2014 for Sentinel-1 synthetic aperture radar with 5 m resolution and in 2015 for Sentinel-2 multispectral instrument at 10 m and 20 m resolution, and 5-days temporal frequency), PlanetScope micro-satellites (3.7 m resolution, available since 2016, and daily temporal frequency) are widely used (Pickering et al., 2021; Li et al., 2020; Potapov et al., 2019; Zhang et al., 2019). Harnessing the high temporal frequency from MODIS and the higher spatial resolution from Landsat along with their long data record is an advantage for improved WC monitoring (Potapov et al., 2008).

Mapping of WC using satellite observation has evolved from discrete to continuous fields (Buchhorn et al., 2020; Hansen et al., 2002). In savanna ecosystems, different cover types (trees, shrubs, and grasses) coexist in single pixels (e.g., at Landsat and MODIS resolution). Finding pure pixels represented by single vegetation type is often difficult and hence discrete classes suffer from accurate representation of variability in such heterogeneous areas. Furthermore, detecting small changes can be hard with discrete classes since changes do not necessarily cause shift from one class to another (e.g., degraded forest might remain forest although WC is less). These and other limitations challenge the accuracy of traditional discrete classification approach and its application for change detection at medium resolution (Sulla-Menashe and Friedl, 2018; Hansen et al., 2002). A shift towards continuous vegetation fields, which are based on regression rather than classification, are providing better representation through estimating fractional cover of vegetation types in a pixel (Hansen et al., 2013; Sexton et al., 2013).

Existing vegetation continuous field (VCF) products such as MODIS VCF (DiMiceli et al., 2015), global forest cover and change (Hansen et al., 2013), and Landsat VCF (Sexton et al., 2013) are mainly suited for monitoring forest, defined as woody vegetation >5 m height. Yet half of EA is covered by savanna and woodlands that are often <6 m tall (Pellikka et al., 2018; Friis et al., 2010; White, 1983). The height threshold in global products under-represents woody vegetation in these ecosystems, despite their major role in ecosystem service provision and carbon budget (Bouvet et al., 2018). For example, the dominant woody vegetation (i.e., Acacia-Commiphora ecosystem) in the region is characterized by shorter trees (3–5 m) (Friis et al., 2010; White, 1983) as compared to height thresholds used in the global products. Recognizing their importance, some countries in EA started incorporating these trees in their operational forest definition for reducing emissions from deforestation and forest degradation and the role of conservation, sustainable management of forests, and enhancement of forest carbon stocks in developing countries (REDD+) and Monitoring, Reporting, and Verification (MRV) implementation (Bekele et al., 2018). For instance, Ethiopia updated forest definition to include trees ≥2 m and minimum canopy cover of 20% (FAO, 2020; Bekele et al., 2018). Hence, improving capability to monitor woody cover change dynamics is important to fill this gap in the region.

Although there are many fractional woody cover change (WCC) studies locally or in selected sites in EA (e.g., Li et al., 2020; Axelsson and Hanan, 2018), only few regional studies that cover wider geographic area and timescale occur (e.g., Hansen et al., 2013; Venter et al., 2018; Brandt et al., 2017; Sexton et al., 2013). While the passive microwave observation studies use vegetation optical depth data (25 km spatial resolution) for estimating WCC (Brandt et al., 2017), the optical satellite observation studies are largely based on machine learning prediction algorithms and Landsat metrics (Hansen et al., 2013; Venter et al., 2018). The predictions are often trained on reference woody cover data from interpretation of very high-resolution imageries (e.g., Hansen et al., 2013) or Google Earth imagery (Venter et al., 2018). In these studies, however, contradicting results were reported over Ethiopia. For example, dominant WC loss from passive microwave observation studies (e.g., Brandt et al., 2017) and dominant WC gain from optical Landsat time series metrics (e.g., Venter et al., 2018). Hence, further studies are required to clarify WCC in this region. In this regard, utilizing Landsat spectral metrics and non-parametric machine learning algorithms trained on a high-accuracy reference woody cover data from airborne laser scanning offers promising prospect (Potapov et al., 2019).

While monitoring WCC based on machine learning algorithms is important, complementing this analysis with breakpoint detection algorithm is highly valuable for detecting major abrupt changes (i.e., intensive WCC hotspots) (De Jong et al., 2013; DeVries et al., 2016; Verbesselt et al., 2010). The algorithms can be parametric and based on piecewise liner model, which are largely used in detecting abrupt change in satellite observation time series (De Jong et al., 2013; DeVries et al., 2016; Verbesselt et al., 2010) or non-parametric and based on permutation test (Zeileis and Hothorn, 2013). Although the non-parametric, distribution-free, methods have better potential in detecting breakpoint in smaller samples (Zeileis and Hothorn, 2013), they are not yet used for similar application using satellite observation.

Despite the important progress made in detecting abrupt changes, application of breakpoint detection algorithms in arid environment (e.g., in EA) still has challenges in detecting WCC associated with site-specific environmental properties and low signal-to-noise ratio in vegetation indices (Schultz et al., 2016; Verbesselt et al., 2010). Hence, testing several methods and applying novel approaches in WC loss hotspot areas is needed to improve the detection of WCC induced by human activities and its application for wider geographic area.

The present research aims to identify major breakpoints and fractional change in WC during 2001–2019 for filling the knowledge gap in WCC detection in regions dominated by shorter trees (3–5 m), which are below the height threshold of most global products of vegetation continuous fields. In addition, the study aims to clarify the controversies in the estimates of WCC in EA. Different from earlier studies of breakpoint detection using satellite observation time series data based on piecewise, parametric liner models, this study presents a non-parametric approach based on permutation test for improved breakpoint detection in WC using MODIS time series. Furthermore, WC prediction models are trained on reference WC data from airborne laser scanning instead of high-resolution imagery to improve WCC monitoring capability in EA. The study covers Ethiopia and Kenya and complements WC predictions with breakpoint detection algorithm to specifically: (1) identify areas affected by abrupt/gradual changes, (2) estimate the net WCC for the corresponding areas affected by abrupt/gradual changes, and (3) identify ecosystems most affected by WC loss and whether those are located near protected areas.

## 2. Study area

The study region is located in Eastern Africa and comprises Ethiopia and Kenya (Fig. 1a). With total surface area of ≈ 1,717,000 km$^2$, the region has a population of around 168 million and is characterized by

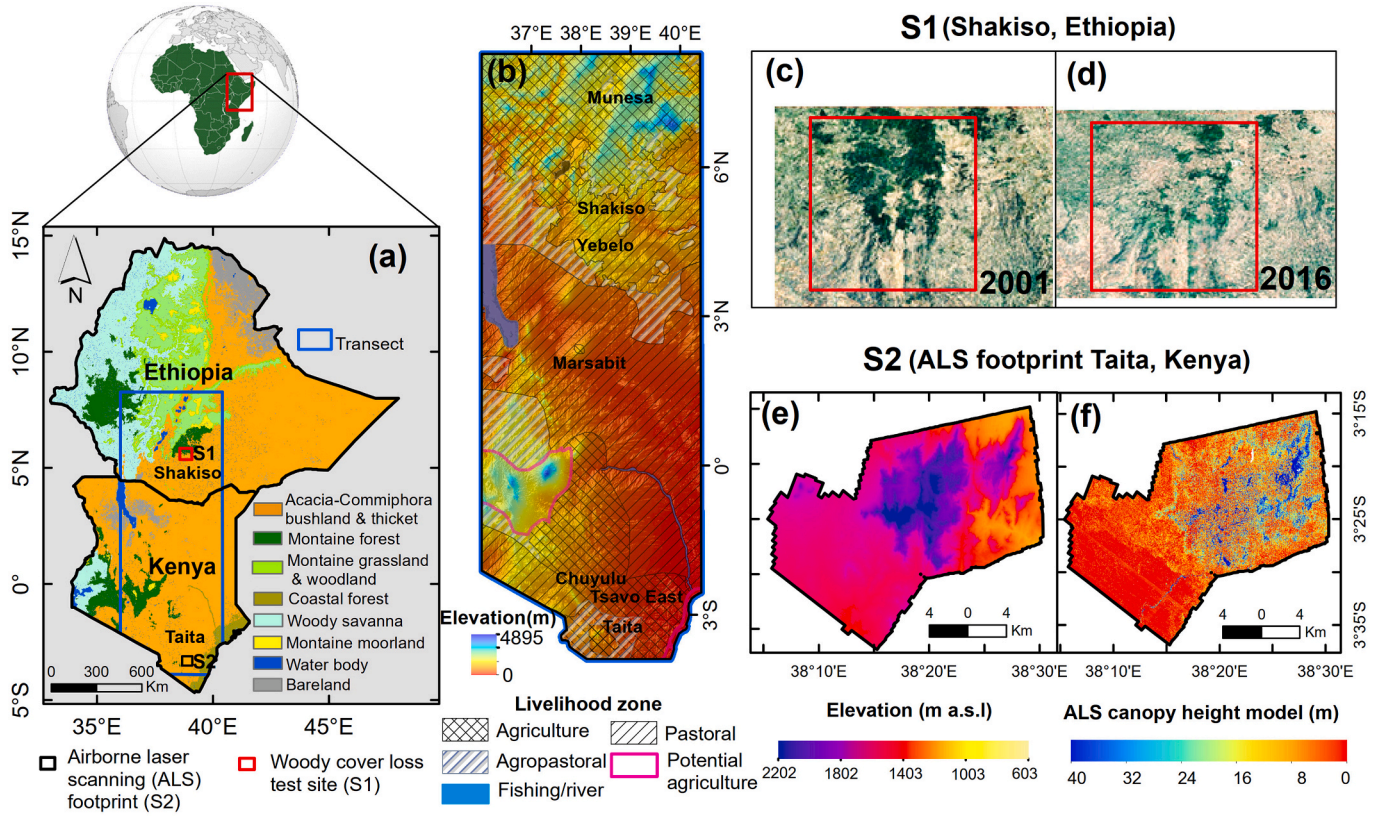


**Fig. 1.** Panels showing: (a) ecoregion map modified from Dinerstein et al. (2017) based on Friis et al. (2010) with location of woody cover loss test site in Ethiopia (S1) and airborne laser scanning (ALS) footprint in Kenya (S2); (b) closer view of elevation (USGS 30 m DEM) and livelihood transect modified from famine early warning systems network or FEWS NET, USAID; (c & d) Google imagery of woody cover at Shakiso town in 2001 and 2016, Ethiopia; e) elevation of the ALS site at 30 m resolution; and f) ALS canopy height model displayed at 30 m resolution in Taita Hills, Kenya.

diverse topography, climate, livelihoods, and ecosystems. Elevation ranges from 125 m below sea level in the Danakil Depression in Ethiopia to around 5199 m above sea level at Mount Kenya summit. While livelihoods in the highlands are mainly based on agriculture, the lowlands are dominated by pastoral livelihood (Fig. 1b). Climate ranges from arid and semi-arid in the lowlands to humid in the highlands of Ethiopia and Kenya.

The region is characterized by multi-modal rainfall pattern and receives up to three rainfall maxima. Apart from northern Ethiopia, which receives unimodal rainfall from June to August, most of the region receives annual rainfall from two seasons: "long rains" from March to May and "short rains" from October to December. Rainfall distribution and variability is affected by local topography, regional convergence zone (e.g., north–south movement of the Intertropical Convergence Zone), and remote climate oscillations (e.g., the Indian Ocean Dipole, El Niño-Southern Oscillation, and the Madden-Julian Oscillation) (Nicholson, 2017).

Influenced by the wide topographic and climatic gradients, the study area is characterized by several ecoregions consisting of various woody vegetation types (Fig. 1a). The Acacia-Commiphora bushlands and thickets (ACBT) ecosystem is the largest and covers approximately half of the entire region. This ecosystem is dominated by 3–5 m tall deciduous bushlands and thickets, and mainly occurs in the arid and semi-arid parts of the region (Abera et al., 2020a, 2020b; Friis et al., 2010; White, 1983). The most characteristic species of ACBT ecosystem are the drought-resistant *Acacia* and *Commiphora* genera (Dinerstein et al., 2017; Friis et al., 2010). Human activities such as fire-wood extraction, charcoal production, and agriculture are the main threats in this ecosystem (Friis et al., 2010).

The Ethiopian montane grassland and woodland (EMGW) or wooded grassland ecosystem occurs in the highlands of either side of Ethiopian's main rift valley (Fig. 1a). EMGW comprises of dry evergreen montane trees and grass complex and the most common tree species include *Juniperus procera and Podocarpus* (Friis et al., 2010). While the woody savanna ecosystem in this paper includes the Sudanian savanna (Western Ethiopia), the Sahelian Acacia savanna (northern and north-western Ethiopia) and Victoria-Basin Forest-savanna (western Kenya) ecoregions (Dinerstein et al., 2017). This ecosystem is characterized by deciduous *Combretum-Terminalia* woodlands with well-developed grass stratum that are susceptible to burning in the dry season (Friis et al., 2010).

The montane forest ecosystem occurs in the highlands of Ethiopia and Kenya (Fig. 1). It is characterized by moist evergreen species with broad-leaved and multi-layered canopies (Friis et al., 2010). While the coastal forest, which belongs to the northern Swahili coastal forest ecosystem, is a moist, semi-deciduous, broad-leaved species and occurs along the Kenyan coast in the south part of the study region (Dinerstein et al., 2017, Fig. 1).

The forest loss test site is located near Shakiso town in southern Ethiopia (Fig. 1a–d). The site (~ 56 km × 55 km) mainly contains montane forest ecosystem. The region is known for its gold mineralization, where the Lega Dembi gold mine is located near Shakiso town (Ghebreab et al., 1992). Site details about local climate and forest loss identification steps are described in Abera et al. (2018). Similarly, the Taita Hills airborne laser scanning (ALS) site comprises montane forest and agroforestry in the highlands, and thickets and bushlands of the ACBT ecosystem and dryland agriculture in the mountain slopes and lowlands, respectively. Being the northernmost part of the Eastern Arc Precambrian mountain chain, similarly as with other montane forest ecosystems, Taita Hills is an important water resource for the lowlands and has high biodiversity (Mittermeier et al., 1998).

## 3. Material and methods

### 3.1. Datasets

Several data obtained from airborne and satellite platforms as well as multiple sources were used in this study. Airborne laser scanning (ALS) data were acquired from several surveys during 2014–2015 (Amara et al., 2020; Adhikari et al., 2016). In all surveys, Leica ALS60 sensor mounted on an aircraft was used. Flying height varied between surveys and due to variable topography from approximately 430 m to 2000 m above ground level. Maximum of four returns per pulse were recorded. As a result, return density varied in the range of 0.5–5 returns/$m^2$ depending on the area (mean 2.8 returns/$m^2$). LAStools software was used to classify ground, vegetation, and building returns and to create digital elevation model (DEM) and canopy height model (CHM) at 1 m resolution. Woody vegetations were retrieved from CHM by applying a 3 m threshold to separate understory and ground returns from woody canopy returns. The CHM is not affected by returns from ground and lower vegetation at this threshold. The threshold matches with the height range (3–5 m) of the dominant ecosystem in the region (Friis et al., 2010; White, 1983). Hence, woody cover in this study refers to fraction of surface area covered by woody vegetation with minimum height of $\geq$3 m. The CHM was processed to estimate canopy cover percentage at 30 m resolution. This data was used for training and validation of woody cover prediction model in section 3.2.1.

Landsat 7 (ETM+) and Landsat 8 (OLI) surface reflectance data were used for predicting fractional woody cover in section 3.2. Spectral bands in visible (Blue, Green, Red), near infrared (NIR) and shortwave infrared (SWIR1 and SWIR2) range were used. Pixels affected by cloud and cloud-shadow as well as Landsat 7 SLC-off gaps were masked using flag bits of the quality assessment band in GEE. To allow consistent temporal continuity of ETM+ and OLI bands, with the latter having a narrower wavelength than the former sensor, a band transformation function (i.e., from ETM+ to OLI bands) were applied using coefficients from Roy et al. (2016).

MODIS nadir BRDF-adjusted reflectance (NBAR) product from collection 6 was used for computing normalized difference vegetation index (NDVI). The NBAR product was accessed and processed on Google Earth Engine (GEE) cloud computing platform (Gorelick et al., 2017). This 500 m resolution combined-product from MODIS Terra and Aqua sensors is prepared at daily time step using directional reflectances corrected for view angle effect (Schaaf and Wang, 2015). Choice of NBAR product over other MODIS products is due to its sensor viewing angle fixed to nadir, avoiding artefacts in NDVI associated with sensor viewing geometry variation (Franch et al., 2013). We used the quality control layer and bit index to retrieve only good quality full BRDF inversion pixels. Frequency of good quality pixels is presented in Supplementary Fig. S1.

NDVI derived from MODIS Multi-angle Implementation of Atmospheric Correction (MAIAC) product (MCD19A3) (Lyapustin and Wang, 2018) was used as input for testing and selecting break point detection algorithms (Supplementary section 3). The product, which is at 1 km resolution and 8-day composite, was downloaded from NASA's Atmosphere Archive and Distribution System (LAADS). MAIAC algorithm – through its advanced cloud detection, aerosol retrieval, and atmospheric correction – provides cloud-free and low aerosol retrievals (Lyapustin et al., 2012). We have corrected the reflectance for the impacts of sun-sensor illumination variation by fixing sensor view angle at nadir and solar zenith angle at 45° using MAIAC Bidirectional Reflectance Distribution Function (BRDF) model parameters.

For experimental testing of break point algorithms, we used CHIRPS (Climate Hazards Group Infrared Precipitation) precipitation data in TSS-RESTREND (Time Series Segmentation and Residual Trend analysis) method. The data was obtained from University of California (https://www.chc.ucsb.edu/data/chirps) at 5 km spatial resolution and monthly timestep.

For analysing drivers of woody cover change, cropland extent, human population, burned area and livelihood data were used. Cropland fraction data at 100 m spatial resolution were obtained from the Copernicus Global Land Service Land Cover 100 m (CGLS-LC100) for the year 2019. This product was prepared from Project for On-Board Autonomy – Vegetation (PROBA-V) time-series, high quality land cover training sites, and ancillary datasets, with an accuracy of around 80% (https://land.copernicus.eu/global/products/lc).

Gridded population of the world (GPW, version 4) data were downloaded from NASA Socioeconomic Data and Applications Center (SEDAC, 2021) (https://sedac.ciesin.columbia.edu/data/collection/gpw-v4). The GPW data are available at 1 km resolution for the years 2000, 2005, 2010, and 2020. The 2010 population and housing censuses data served as a basis to extrapolate population estimates for the other years in GPW v4.

For burned area data, monthly MODIS (MCD64A1 Version 6) product at 500 m resolution was downloaded from NASA Land Processes Distributed Active Archive Center (LP DAAC) (Giglio et al., 2015). Livelihood zone data (i.e., agriculture, pastoral, and agropastoral zone) were obtained from United States Agency for International Development (USAID), famine early warning systems network (FEWS NET) (https://fews.net/east-africa/).

The various data were harmonized spatially to 500 m resolution. Spatial resampling to 500 m resolution was done by applying bilinear interpolation. Daily, 16-day, and 8-day composite data were averaged to monthly value.

### 3.2. Methods

The overall methodology has two main steps (Fig. 2). First, fractional WC was predicted based on ALS, Landsat spectral metrics, and random forest algorithm (Section 3.2.1). Second, pixels affected by abrupt or monotonic WCCs were identified using MODIS normalized difference vegetation (NDVI) (Sections 3.2.2 and 3.2.3). Breakpoint detection algorithms were tested in the forest loss test site to select appropriate method for the study area (Supplementary section 3, Fig. S3). The selected method was used to identify presence of statistically significant abrupt change in each pixel. We were interested in major breaks or a single "most important break" (De Jong et al., 2013) during 2001–2019 as they are important in terms of indicating severe changes in WC. For pixels not affected by abrupt changes, we evaluated the presence of monotonic changes. Next, for those pixels affected by significant ($P < 0.05$) abrupt or monotonic changes, the magnitude of WCC was estimated from the trends of predicted fractional WC. Details of each step are presented in the below sections.

#### 3.2.1. Fractional woody cover prediction and change

For areas affected by significant monotonic change or abrupt change, WC was predicted for each pixel applying Random Forest (RF) model in GEE. Reference WC data for the RF model were obtained from airborne laser scanning (ALS) and predictor variables consisting of Landsat (7 and 8) spectral-temporal metrics.

Spectral metrics and various vegetation indices (Table 1) were computed using Landsat 7 (ETM+) and Landsat 8 (OLI) as predictors for the RF model in GEE. Second, median dry season composites were computed for the selected bands. Vegetation indices including NDVI, enhanced vegetation index (EVI), soil adjusted vegetation index (SAVI), reduced simple ratio (RSR), and tasseled cap greenness (TCG, see Baig et al., 2014 for coefficients) were used. These indices are commonly used for predicting woody cover fraction (Venter et al., 2018; Adhikari et al., 2016). While NDVI and TCG are used as they highlight vegetation greenness, the others (EVI, SAVI, and RSR) are included as they provide enhanced vegetation signal by supressing background effect on canopy reflectance (Huete et al., 2002; Brown et al., 2000; Huete, 1988). Ratios of spectral bands were also used as these are less sensitive to topographic effect.

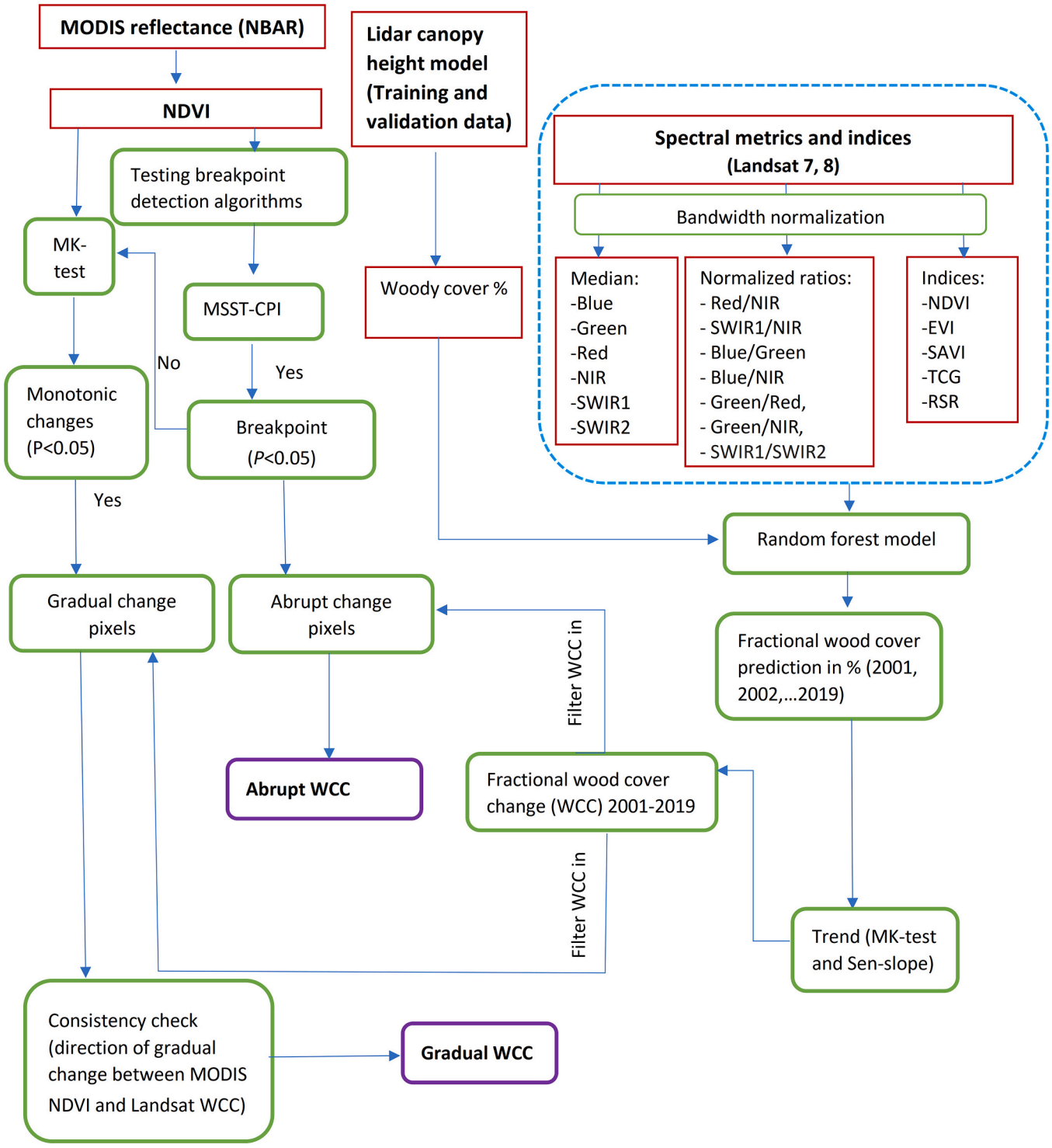


**Fig. 2.** Methodology flow diagram. NBAR = nadir BRDF-adjusted reflectance; NDVI = normalized difference vegetation index; MSST-CPI = Maximally Selected Statistics Tests - Conditional Permutation Inference; MK = Mann-Kendall; NIR = near infrared; SWIR = shortwave infrared; EVI = enhanced vegetation index; SAVI = soil adjusted vegetation index; TCG = tasseled cap greenness; RSR = reduced simple ratio.

Third, the RF model was built and validated at the ALS footprint site (Fig. 1a, e, f) for year 2015 and used to extrapolate the ALS WC to the entire study area. For this, a total of 7000 stratified random sample points were generated. Stratification was done using ALS WC at 10% interval (i.e., 0–10% up to 90–100%). From each WC bin, 700 random samples were generated. We used 70% (4900 points) for model training and internal cross-validation and 30% (i.e., 2100 points) for independent or external validation. The RF regression model was run using these parameter settings (number of trees = 500, variables per split = 6, and node size = 5).

The model produced moderate performance, explaining 66% (internal accuracy on the training data, $r^2$ = 0.66 and root mean square error (RMSE) = 16%) and 68% (external accuracy on the testing data, $r^2$ = 0.68 and RMSE = 13.7%) of the WC variance in the ALS data (Fig. 3a–c). The importance of predictor variables was quantified using mean decrease in accuracy (%IncMSE) (Supplementary Fig. S4). This

**Table 1**
Spectral metrics and vegetation indices derived from Landsat (7 and 8). NIR = near infrared; SWIR = shortwave infrared; NDVI = normalized vegetation index; EVI = enhanced vegetation index; SAVI = soil adjusted vegetation index; RSR = reduced simple ratio; TCG = tasseled cap greenness.

| Predictors | Metrics/Formula |
|---|---|
| Surface reflectance | Dry season median: Blue, Green, Red, NIR, SWIR1, SWIR2 bands<br>Ratios: Red/NIR, SWIR1/NIR, Blue/Green, Blue/NIR, Green/Red, Green/NIR, SWIR1/SWIR2 |
| NDVI | NIR–Red/ NIR + Red |
| EVI | 2.5 × (NIR – Red) / (NIR + 6 × Red – 7.5 × Blue +1) |
| SAVI | (NIR – Red) × (1 + 0.5) / (NIR + Red+0.5) |
| RSR | (NIR/Red) × ($SWIR1_{max}$ – SWIR1) / ($SWIR1_{max}$ – $SWIR1_{min}$) |
| TCG | −0.2941 × Blue – 0.243 × Green – 0.5424 × Red +0.7276 × NIR + 0.0713 × SWIR1–0.1608 × SWIR2 |

model was then used to predict WC for each of the years 2001–2019. Finally, the magnitude of WCC was computed from the trends of the predicted WC, which was detected by MK test, for every pixel affected by significant ($P < 0.05$) abrupt or monotonic changes using Sen's slope (Wilcox, 1998). Sen's slope is a non-parametric test and an alternative to parametric linear regression. It is robust to outliers because the median slope is used instead of calculating a mean slope as in parametric tests.

To increase the consistency and reliability of result across sensors (MODIS and Landsat), only pixels that showed agreement in the direction of trends (i.e., increase or decrease) between monotonic changes from MODIS NDVI and WCCs from machine learning algorithm were considered. Pixels that showed disagreement in the direction of change (e.g., pixels showing an increase in gradual change in MODIS NDVI and a decrease in WCC) were approximately 5% and masked from all analysis.

### 3.2.2. Breakpoint detection in woody cover

To detect abrupt (or interrupted) changes in vegetation, a novel approach based on non-parametric conditional permutation inference (CPI) was applied on the NBAR derived NDVI using Maximally Selected Statistics Tests (MSST) from "Coin" Package in R (Hothorn et al., 2008). CPI approach has a better power in detecting breaks in smaller number of observation than the asymptote inference approach (Zeileis and Hothorn, 2013).

Unlike the asymptotic break detection methods, such as Breaks For Additive Seasonal and Trend or BFAST (Verbesselt et al., 2010) and its derivatives (e.g., Time Series Segmentation and Residual Trend analysis (TSS-RESTREND), Burrell et al., 2017), MSST test the independence of data distribution between two sets of variables ($Y_i$ = short-dry season median NDVI and $X_i$ = time; $i$ = 2001, …,2019) and identify best cut point using maximally selected test statistics ($T_{max}$) based on permutation inference (Zeileis and Hothorn, 2013; Hothorn and Zeileis, 2008).

This is done in two steps. First the null hypothesis, which states that the distribution of response variable $Y_i$ is independent of the covariate $X_i$, is tested against cut point alternatives where the distribution of the response variable varies between two groups of observations ($Y_i$) with respect to $X_i$. Cut point alternatives, which range between 0 and 1, are calculated from quantiles of $X_i$. All possible cut points into two groups are evaluated, ordering by $X_i$. Second, the best cut point or break point are selected. For this, the test statistics (T) are standardized to common scale and the best separating cut point is the one with the maximum value of standardized statistics (Tmax) (Eqs. 1–4). Details of the algorithm are provided in Hothorn et al. (2008).

$$\mathrm{Tmax} = max\frac{|\mathrm{T}-\mu|}{\sqrt{diag(\mathrm{M})}} \tag{1}$$

$$\mathrm{T} = \mathrm{vec}\left\{\sum_{i=1}^{n} g(\mathrm{Xi})h(\mathrm{Yi})^{\mathrm{T}}\right\} \in \mathrm{R}^{pq\times 1} \tag{2}$$

where μ is mean; M is covariance matrix; h is an influence function applied to the response $Y_i$ (i.e., $h: Y \rightarrow R^{q\times 1}$) and g is a set of candidate cut points or partitions (p) defined by $g(X) = \{g_1(X), \ldots, g_p(X)\}$; vec is an operator which stacks the columns of a matrix.

$$\mu = \mathrm{E}(\mathrm{T}|\mathrm{S}) \in \mathrm{R}^{pq\times 1} \tag{3}$$

$$\mathrm{M} = \mathrm{V}(\mathrm{T}|\mathrm{S}) \in \mathrm{R}^{pq\times pq} \tag{4}$$

where μ and M are obtained by conditioning on all possible permutations (S) of the response variable $Y_i$ ($i$ = 2001, …, 2019) under null hypothesis; E is the conditional expectation.

Reference conditional distribution of test statistics was computed directly from the data without any distributional assumption. For this, we used a conditional Monte Carlo procedure in MSST from all admissible permutations of the response variable. To detect presence of statistically significant ($P < 0.05$) break in short-dry season NDVI median composites from 2001 through 2019 (i.e., maximum of 19 sample points for each pixel)

### 3.2.3. Monotonic trend detection

For identifying direction of monotonic (or gradual) changes in WC, NDVI calculated from MODIS NBAR product was used. Significant monotonic changes were identified using non-parametric Mann-Kendall trend test (Kendall, 1975; Mann, 1945) (Eqs. 5–7).

For better detection of WCCs, we used short-dry season (January and February) median NDVI, which has the best contrast between woody

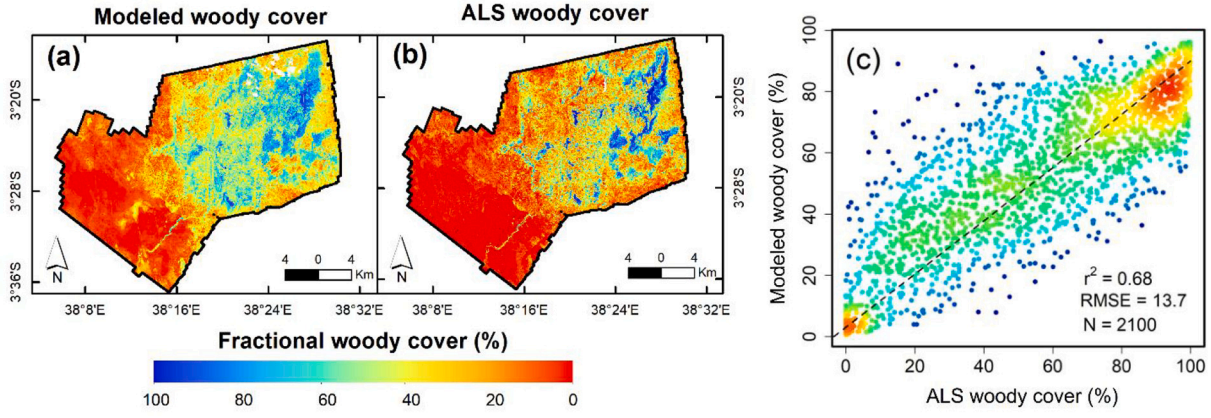


**Fig. 3.** Spatial distribution of (a) fractional woody cover predictions based on random forest model, (b) fractional woody cover estimates from airborne laser scanning (ALS) data in Taita Taveta County, Kenya, and (c) the comparison between the two.

cover and herbaceous grass cover (Borges et al., 2020). In this season, leaves remain intact in comparison to the leaf-off situation in the long-dry season from mid-May to September (see details about phenology of the dominant *Acacia-Commiphora* trees in Fenner, 1982). Impact of herbaceous cover (e.g., grasses) on the vegetation indices is minimal in dry season compared to wet season as precipitation masks woody changes through enhanced vegetation productivity (Abera et al., 2018). A comparison of monotonic trends in a known forest loss site (Shakiso, Supplementary Fig. S2) further showed a clear advantage of using short-dry season than wet season composite for capturing WCCs in the region.

$$S = \sum_{i=1}^{n-1} \sum_{j=n+1}^{n} sgn(X(j) - X(i)) \quad (5)$$

$$\begin{cases} sgn(X) = 1 \text{ if } X > 0 \\ sgn(X) = 0 \text{ if } X = 0 \\ sgn(X) = -1 \text{ if } X < 0 \end{cases} \quad (6)$$

where S = test statistics; X = short-dry season median NDVI time series (2001–2019); sgn = signum function; n = length of time series. A positive and negative value of *S* indicates an upward and downward trend, respectively. The mean of S is $\mu = 0$ and the variance var. (S):

$$var\,(S) = \frac{1}{18}\left(n(n-1)(2n+1) - \sum_{i=1}^{p} t_j i(i-1)(2i+5)\right) \quad (7)$$

where p is the number of tied groups and $t_j$ is the number of data points in the i-th tied group. The null hypothesis, which is there is no trend, is rejected if the absolute value of standardized test statistics (*Z*) is bigger than the theoretical value ($Z_{1-\alpha/2}$), where $\alpha$ is the statistical significance level.

#### 3.2.4. Exploratory analysis on causes of woody cover change

To identify relation of WCC with anthropogenic (cropland expansion, livelihood, and population growth) and natural factors (fire), a simple exploratory analysis method is presented. Spatial association between cropland expansion and WC change was explored using 2019 cropland fraction data from Copernicus CGLS LC100. The spatial association was assessed by first masking cropland extent with WCC result and computing summary statistics on percentage of WC replaced by cropland pixels. The association was further explored by superimposing livelihood zone data from FEWS NET.

For assessing relation between WCC and population growth, population data from GPW was used. Since data are available for the only years 2000, 2005, 2010, and 2020, we linearly interpolated the remaining years, computed 2001–2019 population density trend, and intersected with WCC.

Relation of naturally occurring fire events with WCC was assessed using MODIS burned area data. For this, first fire frequency was calculated for each pixel by converting burn date into binary (i.e., 0 = no fire detected; 1 = fire detected). The fire frequency data were then masked by WCC to identify their links in the region.

## 4. Results

### 4.1. Pixels affected by abrupt or gradual woody cover changes

The total area affected by abrupt WCCs between 2001 and 2019 was 3% larger than areas affected by gradual changes (Fig. 4). From the total surface area of the study region (≈ 1,717,000 km$^2$), significant ($P <$

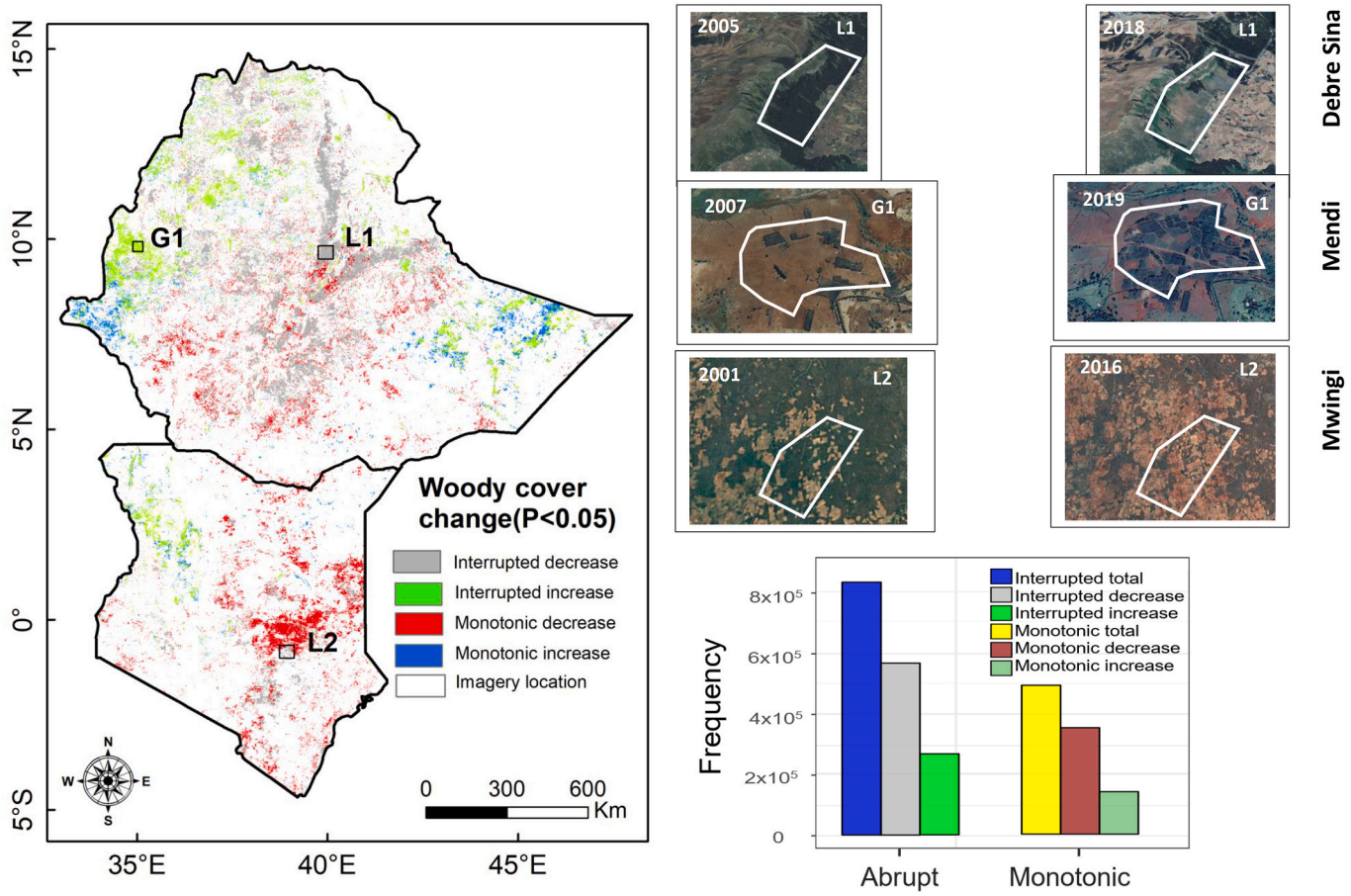


**Fig. 4.** Abrupt and gradual woody cover changes during 2001–2019. Only significant breaks and monotonic trends are displayed.

0.05) abrupt changes accounted for approximately 8%. Of these, 6% showed interrupted decrease and 2% interrupted increase (Fig. 4). On the other hand, around 5% of the study region exhibited gradual or monotonic changes. Of this, 4% experienced monotonic decrease and the remaining 1% increase. High resolution Google imageries show evidences of WC increase (e.g., panel G1 in Medni, Ethiopia) and decrease (e.g., panel L1 in Debre Sina, Ethiopia, and panel L2 in Mwingi, Kenya) in these sites.

### 4.2. Fractional woody cover change

For pixels that have experienced significant abrupt or monotonic changes, the WCC from 2001 through 2019 is presented for every pixel across the study area (Fig. 5b, c). The overall result showed net loss of WC in the study region. Over the 19-years (2001–2019), the region experienced a total WC loss of 21,432 km$^2$ area. Of this, abrupt WC losses accounted for ~59% and gradual losses ~41% (Fig. 5c). The WC loss rate varies across the region with the maximum being around 5% per year. On the other hand, the total WC gain was relatively small in area (5168 km$^2$) with larger contribution (64%) coming from areas of abrupt changes than gradual changes. The maximum rate of gain was 2.6% per year, which was approximately two-times smaller than the maximum rate of loss. Overall WCC were highly dominated by loss (i.e., total loss was >4-times higher than total gain) leading to net loss of 16,264 km$^2$.

### 4.3. Timing of the occurrence of abrupt woody cover changes

Around 72% of the abrupt WCCs observed in our study area occurred between 2002 and 2010 (Fig. 6). During this period, the strongest changes happened in 2008 (13%), 2007 (12%), and 2010 (11%). The remaining 28% occurred between 2011 and 2017 with a declining trend since 2011. The changes in the first three years of the 2011–2017 period were more widespread (20%) than towards the end, where areas affected by abrupt changes reduced considerably (< 1%) in 2017.

The direction of WCC can be negative (e.g., loss due to clearing of woody vegetation for agriculture) or positive (e.g., gain in cases of afforestation or reforestation), and thus timing of break years were analyzed separately for WC loss and gain areas (Fig. 7). The result showed that intensive woody cover loss happened mainly in 2007 and 2008 (each ~16%), 2010 (13%), and 2004 (12%), and strongly declined after 2010. Whereas significant ($P < 0.05$) breaks from woody cover gains were detected during 2006 (17%), 2012 (15%), and 2013 (14%), and declines afterwards. Except in 2006, breaks were dominated by loss between 2002 and 2011 (i.e., clearing of woody vegetation were prevalent throughout this period). By contrast, breaks due to significant woody cover gain dominated since 2012 except for 2016, where gain and loss were comparable in extent.

### 4.4. Woody cover loss hotspots near protected area

A closer view on woody cover loss hotspots near protected areas is displayed in Fig. 8. Woody cover clearing was intensified near Meru National Park in central Kenya over the last 10-years (2009–2019), mainly due to agricultural expansion (Fig. 8b1–b3). Similarly, near Tsavo East National Park, adjacent Athi river in east of Kibwezi town in southern Kenya, agriculture spread extensively at the cost of woody cover between 2002 and 2012 (Fig. 8c1–c3).

In Ethiopia, woody cover clearings inside and outside protected areas were identified (Fig. 8d, e). In Bore-Anferara forest reserve, WC loss occurred during 2001–2019 (Fig. 8d1–d3). The loss could be related to logging as evidence of agricultural actives are lacking from closer investigation of imageries. The Shakiso WC loss test site, which is described in section 2 (see high resolution imageries in Fig. 1c, d), is located ~16 km south of Bore-Anferara forest reserve boundary. Agricultural and mining activities are related to the clearing of WC in Shakiso (see Supplementary Fig. S7).

Additional WC loss hotspot was identified between two national forest reserves in Ethiopia (Fig. 8e1–e3). The hotspot is located ~9 km east of Kenicho town in Ethiopia, within 30 km radius from boundaries of Bulki-Melakoza and Gidole-Kemba national forest reserves. Extensive clearing of WC took place between 2009 and 2017 associated with agricultural expansion in the region.

Woody cover loss hotspots and corridor were compared against

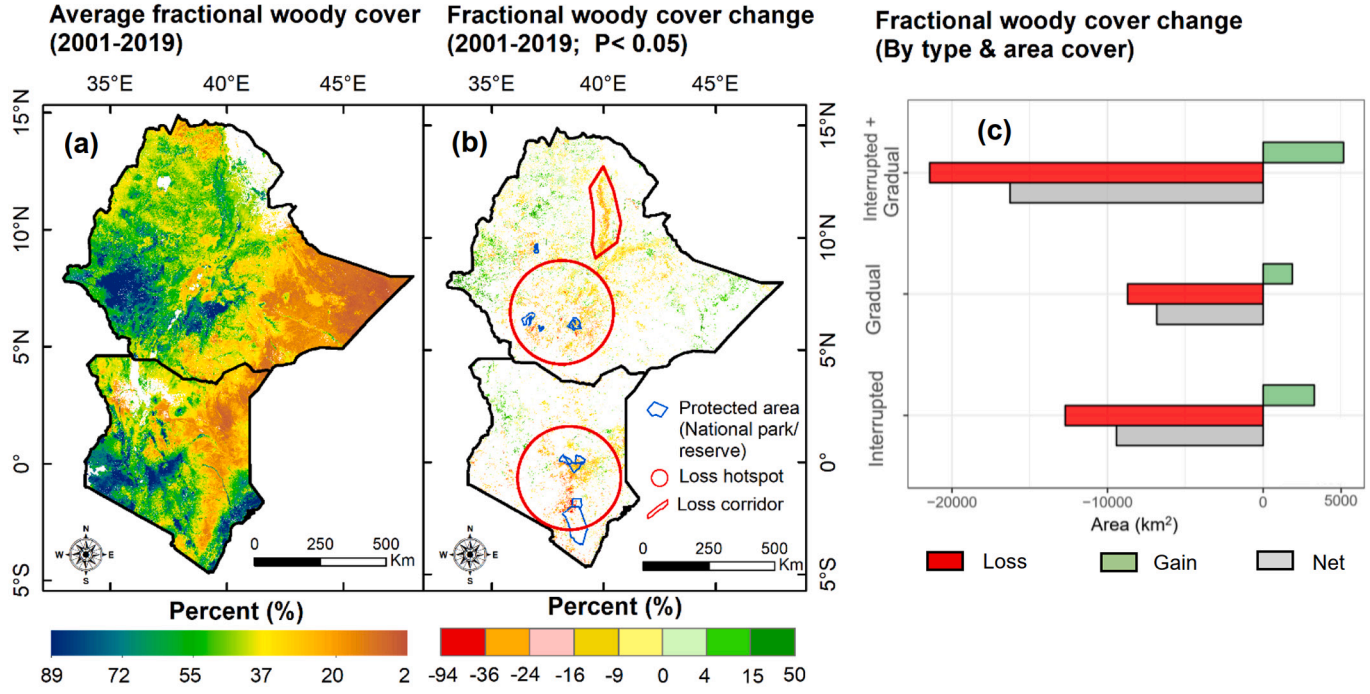


**Fig. 5.** Panel showing (a) average predicted fractional woody cover during 2001–2019, and (b) fractional woody cover change over the last 19-years. Only significant ($P < 0.05$) changes are displayed. Protected area boundaries (i.e., national parks and forest reserves) are from World Database on Protected Areas (WDPA).

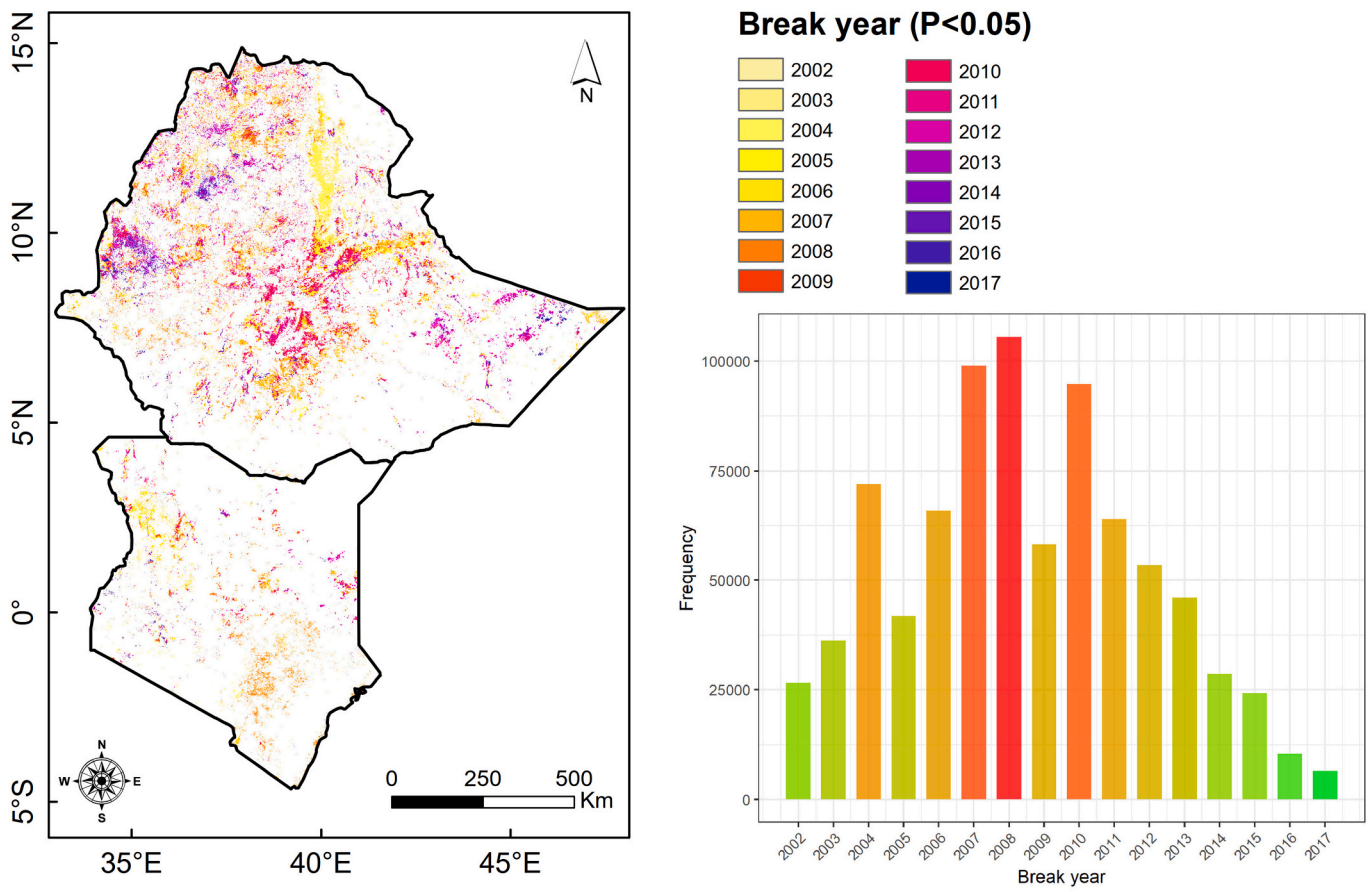


**Fig. 6.** Spatial distribution of the timing of major breaks in woody cover time series during 2001–2019.

global forest loss product from Hansen et al. (2013) (Fig. 9). More areas that have experienced loss were identified by the prediction of ours than the global product by Hansen et al. (2013) between 2001 and 2019. For example, in southern Ethiopia, the total number of pixels with at least 5% woody cover loss were 7-times higher than the global product estimate, considering both abrupt and gradual losses. When accounting losses to abrupt changes only, the estimate is 4-times higher. Similarly, strong underestimation of woody cover loss by global product was prominent in northern Ethiopia and southern Kenya when compared to the predicted loss (Fig. 9b, c).

### 4.5. Fractional woody cover change across ecosystems

To identify ecosystems facing considerable WCC, the result was analyzed per ecosystem type. We observed net loss in all biomes (Fig. 10). Particularly the ACBT ecosystem was the most threatened and exhibited the highest net loss (4.7%), followed by montane forest (2.7%) and montane grassland and woodland ecosystem in Ethiopia (2.5%) (Fig. 12). In terms of total woody cover loss area ($km^2$), 69% of the total loss occurred in ACBT ecosystem in the region, 12% in montane forest, and 11% in Ethiopian montane grassland and woodland ecosystem (see Supplementary Fig. S5 for WC loss area in $km^2$ across ecosystems).

The smallest net loss (1.1%) occurred in wooded savanna, which is mainly located in western Ethiopia, and contributed to 8% of total WC loss area in the region. Relatively more WC gain occurred in savanna ecosystem than in others. While the contributions of abrupt and gradual changes to net loss were comparable in ACBT ecosystem, abrupt losses were dominant over gradual losses in the rest of ecosystems.

### 4.6. Causes of fractional woody cover change

The total contribution of cropland expansion to the WC loss was estimated using spatial association between WCC and 2019 cropland extent (Fig. 11a). Based on the ratio of cropland area to the total WCC area, the contribution of cropland expansion was around 57% during 2001–2019. This is equivalent to around 3% per annum assuming a linear rate of change.

The spatial association between WCC and livelihood zone map further indicated intensive woody cover loss concentrated mainly in agricultural areas close to agropastoral/pastoral zones (Fig. 11b). The North-South running WC loss corridor in Ethiopia and the hotspot in Kenya are located in agricultural lands near pastoral zones. Similarly, the WC hotspot in Ethiopia occurred near both agropastoral and pastoral zones. The result show that WCs in those areas are under intense pressure coming from multiple livelihoods.

Links of WC loss hotspots with population growth and fire frequency is presented in Fig. 12. Areas having high population growth rate overlap with WC loss hotspots largely in Ethiopia and partially in Kenya, indicating possibility of population pressure on WC (Fig. 12a). While the distribution of fire frequency showed that the impact of fire in inducing WC loss was minimum (Fig. 12b). Around 82% of the total area affected by abrupt WCC had zero fire occurrence. Particularly, the WC loss hotspots were the least affected by fire incident and the remaining 18% mainly clustered in the savanna ecosystem in western Ethiopia.

## 5. Discussion

Changes in WC were dominated by net loss across ecosystem during 2001–2019. Compared to previous studies, which reported contrasting result over Ethiopia (e.g., dominant loss in Brandt et al. (2017) and

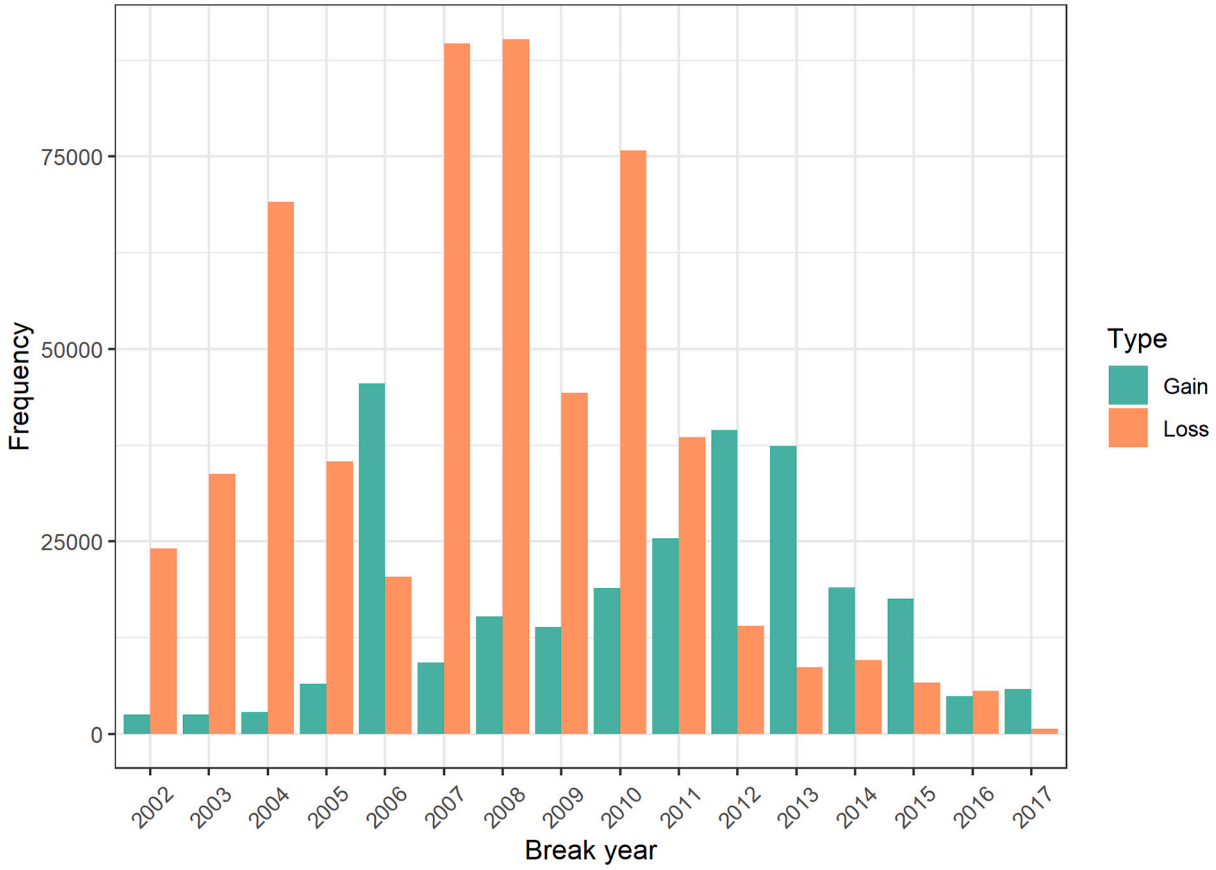


**Fig. 7.** Frequency of break years classified by woody cover loss and gain pixels.

dominant gain in Venter et al. (2018)), our results agree with those studies reporting dominant loss (Brandt et al., 2017). However, in terms of the spatial extent and location of WC loss, there are small inconsistencies that could arise from differences in data (type and resolution), method, and length of analyzed periods used among studies. Over Kenya, there is relatively better agreement between our results and previous studies (e.g., Brandt et al., 2017; Venter et al., 2018).

Despite the net WC loss, different spatio-temporal patterns emerged in 2001–2019. The spatial patterns revealed WC loss hotspots. The hotspots are mainly concentrated in Acacia-Commiphora ecosystem as also identified by a fine-scale study by Pellikka et al. (2018) in Taita Hills, Kenya. Particularly their occurrence in this ecosystem needs further attention. First hotspots are marked by major abrupt change that might signal severe ecosystem degradation and beginning of turning points or irreversible changes. Second, *Acacia-Commiphora* trees provide important socio-economic (e.g., as sources of livelihood through gum, resin, woodfuel provision) and environmental values (e.g., food source and habitat for organisms, improves soil fertility, and modulates climate, etc) (Mesfin and Menbere, 2020; Abera et al., 2020a) and hence sustaining ecosystem service provision from these trees is important in the region. Third, the hotspots are located adjacent or in some places inside protected areas (Figs. 8 and 9), which have global importance in terms of carbon stock, biodiversity and wildlife protection (Mesfin and Menbere, 2020; Bouvet et al., 2018), although in places protected areas also have negative consequences (Amara et al., 2020).

The temporal pattern exhibited contrasting trends of loss and gain after 2010. While WC loss showed a gradual decrease and slowing down of intensive clearing, WC gain exhibited an increase in recent decade. This divergent temporal pattern could be attributed to several factors. The observed temporal pattern in the recent decade (2011−2020) match with the approval and onset of global initiatives such as REDD+ program in Ethiopia and Kenya (Bekele et al., 2018; Bernard et al., 2014). Although the REDD+ initiatives in these countries are still ongoing and establishing direct link to the observed WCC patterns require detailed investigation, the awareness created at high level could have a cascading effect locally and these could contribute to the contrasting patterns obtained. Furthermore, government strategies that support green economy can contribute to this end. For instance, the 2011 Ethiopia's Climate Resilient Green Economy (CRGE) strategy, which aims in building an economy low in its greenhouse gas emissions and avoid natural resources degradation, can help in curbing WC loss and promote afforestation/reforestation and restoration in the region (Bekele et al., 2018; Kassa et al., 2017). Similarly, the 2009 Agriculture (Farm Forestry) Rules of Kenya, which stipulates a farm tree cover of at least 10% of any agricultural land, can promote WC increase in the region (Pellikka et al., 2018).

### 5.1. *Anthropogenic causes of fractional woody cover change*

Clearing of woody vegetation for agriculture is one of the main direct causes of abrupt changes in WC in East Africa (Brink et al., 2014; Figs. 8,11). In line with previous studies, our regional analysis showed important contribution of cropland expansion (57%) to WC loss associated with existing livelihood. The remaining unexplained portion (43%) can be induced by different factors.

Wood fuel (firewood and charcoal) extraction is an important anthropogenic factor that can induce WC loss in the region. Wood fuel accounts for >80% of household energy supply in Ethiopia (UNEP, 2016) and > 70% of national energy need in Kenya (Githiomi and Oduor, 2012). Woody vegetation, particularly Acacia trees, are main sources of charcoal production in the region. Production of charcoal, for example from Acacia, consumes 6-times more wood than its actual

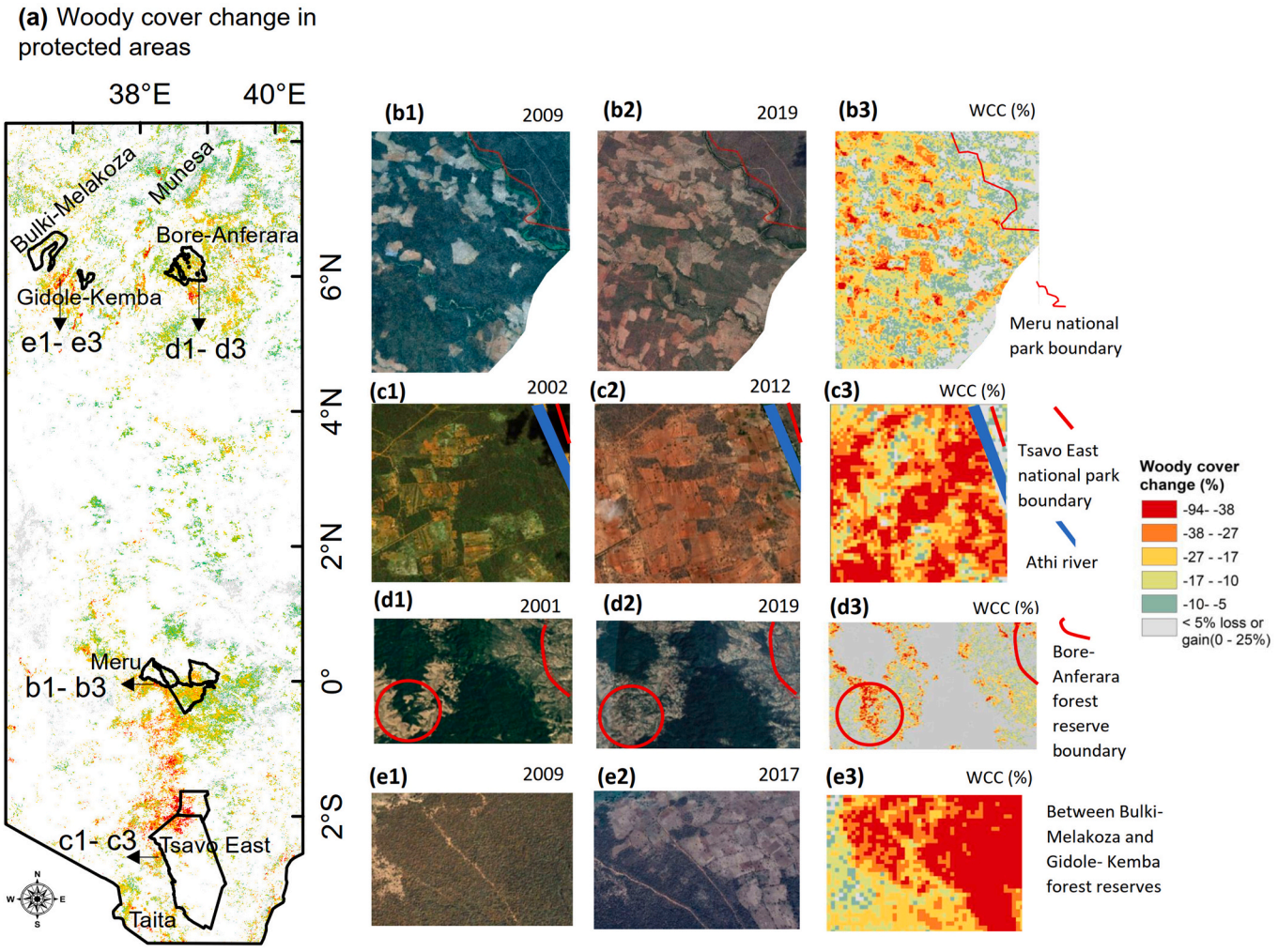


**Fig. 8.** Woody cover loss hotspots and fractional woody cover change (WCC) inside and near protected areas in Kenya and Ethiopia. Panel (a) shows closer view of WCC and location of hotspot sites with protected areas displayed in black. Panels (b and c) show Google imagery and WCC with national park boundary highlighted red in Meru (b1–b3) and Tsavo (c1–c3), Kenya, and in Bore-Anferara forest reserve (d1–d3) and between Bulki-Melakoza and Gidome-Kemabin national forest reserves (e1–e3) in Ethiopia. (For interpretation of the references to colour in this figure legend, the reader is referred to the web version of this article.)

weight (Vuorinen et al., 2016). Hence, in addition to pressure from cropland expansion, the stronger reduction in WC in Acacia-Commiphora bushland and thicket (ACBT) ecosystem can be related to the huge demand for wood fuel in the region, which grows at a rate of 3% per year (Iiyama et al., 2014). While other factors such as cattle grazing land expansions could have important impact on WC loss, role of settlement or urbanization, timber logging, construction (e.g., dams, airports, etc), mining activities (Supplementary Fig. S7) were likely smaller (Vuorinen et al., 2016). Locally, it was also shown in Amara et al. (2020) that protected areas have less woody cover compared to non-conserved areas in lowlands of Taita Taveta County, Kenya. Over the past decade, protected areas as such are not expanding but improved wildlife protection has seen growth in populations of key species such as elephants. The wildlife increment, together with agricultural expansion, has posed a growing pressure on woody cover, leading to an escalation of conflict between people and wildlife (Munyao et al., 2020).

Population growth is considered the underlying driver behind the anthropogenic factors in the region (Brandt et al., 2017). Our results showed spatial link between WCC hotspots and population growth and support earlier findings. Particularly, with high population growth rate in the region (> 2% per year), demand for more crop production and wood fuel increases in the future and this could lead to accelerated deforestation and degradation (UNEP, 2016).

### 5.2. Natural causes of fractional woody cover change

The role of fire in inducing WCC was minimum in the study region. WC loss hotspot occurred mainly in Acacia-Commiphora ecosystem, which are tolerant to fire (Mesfin and Menbere, 2020). High frequency of fire incidents were rather observed in areas of WC gain in savanna ecosystem in western Ethiopia (Fig. 12b; Fig. 1a). The naturally occurring fire in savanna ecosystem, which is dominated by deciduous *Combretum-Terminalia* woodlands and grasslands, is associated with the frequent burning of the perennial grass stratum that are susceptible to fire (Friis et al., 2010). The grasses sprout again after burning and this process increases the frequency of fire by providing new biomass that can burn again (Friis et al., 2010; van Breugel et al., 2016). This in turn could favour WC gain by reducing competition from the grass stratum and might increase *Combretum–Terminalia* woodlands in Western Ethiopia associated with fire-regime (van Breugel et al., 2016).

Climate induced changes can affect fractional WC. Whether this had an impact on WC loss was assessed using the association between frequency of drought and frequency of break years (Supplementary Figs. S6a, b). When maximum number of WC breaks occurred in 2008 and 2007, frequencies of drought-affected areas were minimum for the corresponding years in the region. This could indicate that droughts had small role in inducing abrupt WC changes in the region.

The dominant *Acacia-Commiphora* tree species in this arid region are

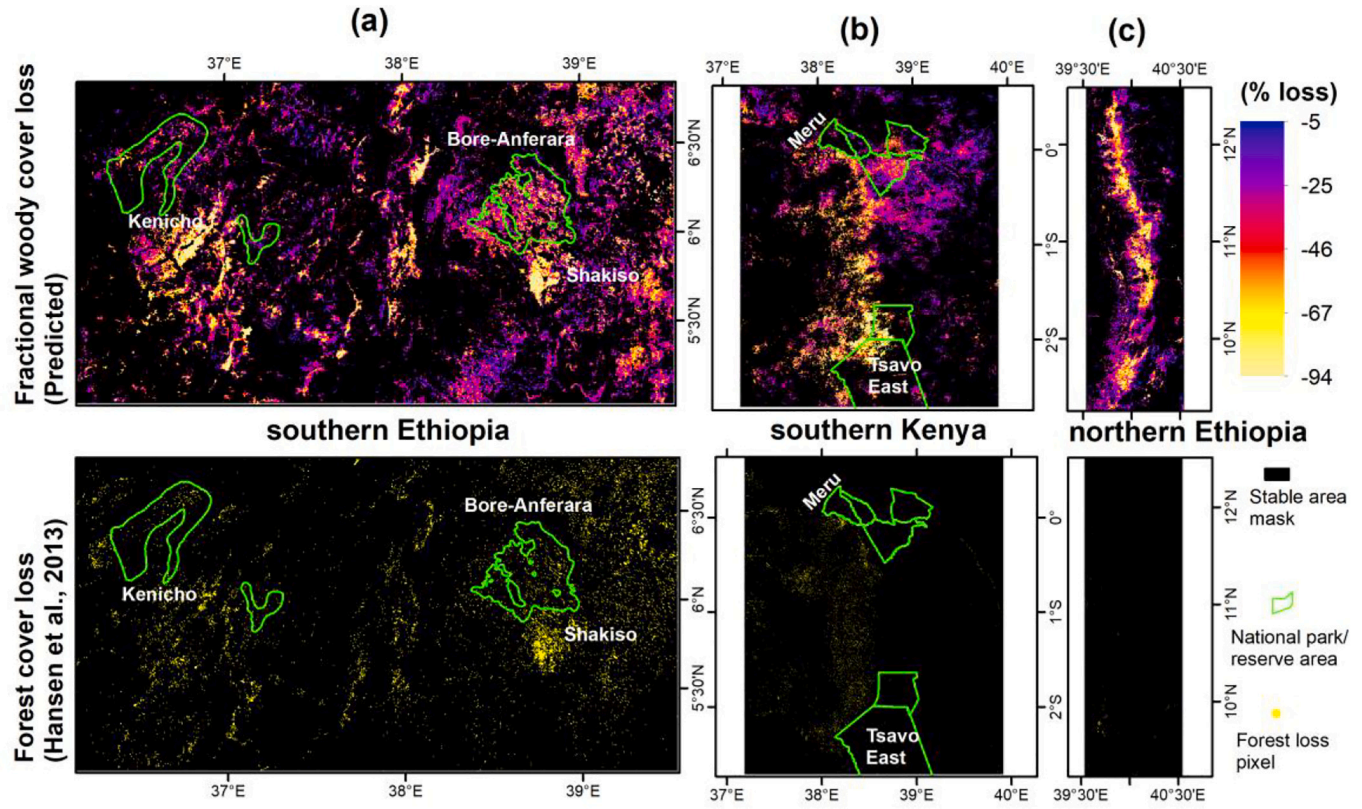


**Fig. 9.** Comparison of global forest loss product (Hansen et al., 2013) and predicted fractional woody cover loss during 2001–2019 over hotspot regions in Ethiopia and Kenya. Protected area boundaries are from World Database on Protected Areas (WDPA). Only protected areas near loss hotspots are displayed.

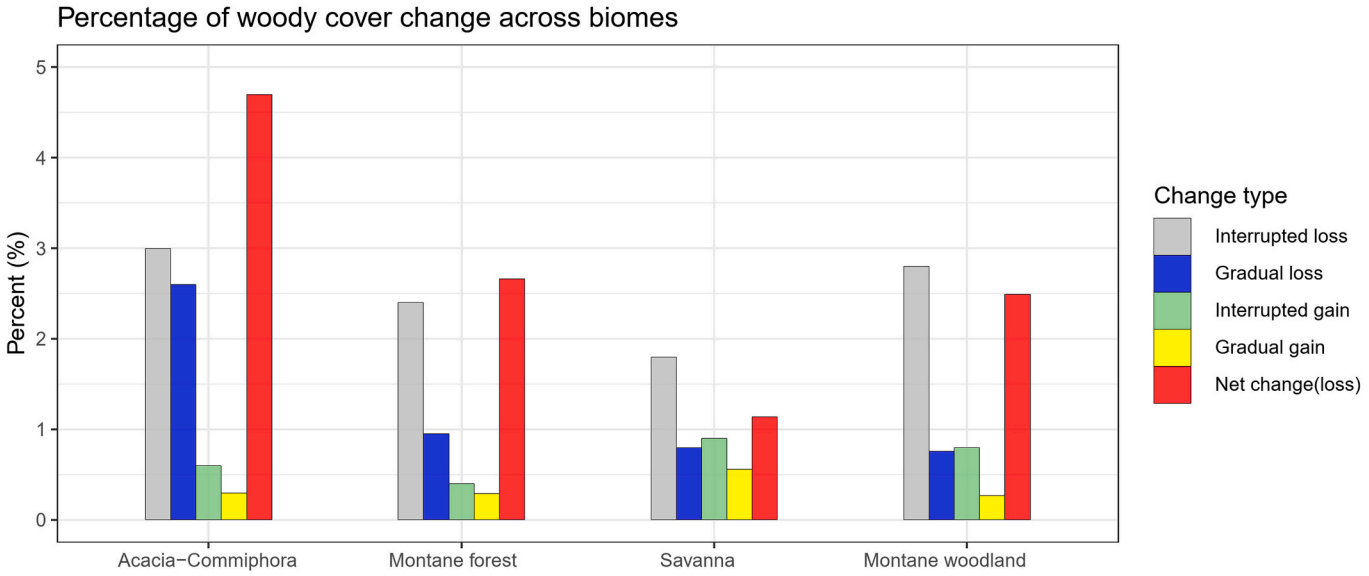


**Fig. 10.** Woody cover change (%) across four ecosystems (Acacia-Commiphora bushland and thicket or ACBT, montane forest, woody savanna, and Ethiopian montane grassland and woodland) in 2001–2019.

tolerant to droughts (Friis et al., 2010). In addition, evergreen forests in East Africa are less sensitive to drought events (Abera et al., 2020b; Abera et al., 2018) as they regulate water loss through stomatal closure and are able to access sub-surface water using their deep rooting systems (Kramer and Boyer, 1995). In times of severe and prolonged drought, however, forests can be vulnerable to hydraulic failure and tree mortality may occur (Williams et al., 2012; Choat et al., 2012). Nonetheless, whether this has occurred in the region and its links to WC loss require further studies.

### 5.3. *Limitations, uncertainties, and future directions*

Although our approach and results demonstrated improved detection of breakpoints and prediction of WC, there are limitations and

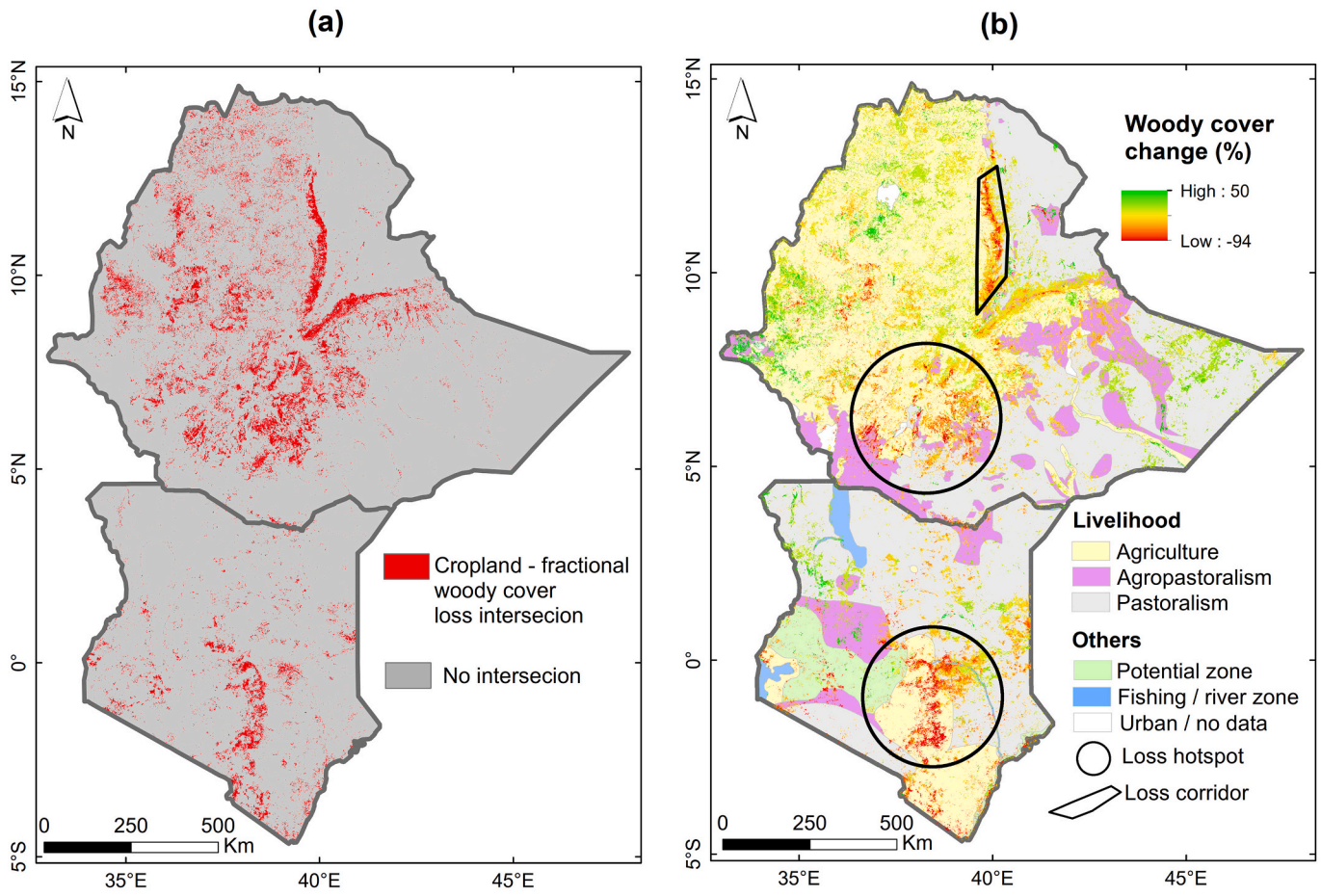


**Fig. 11.** Spatial association of fractional woody cover change with (a) cropland extent from the Copernicus Global Land Service Dynamic Land Cover Map (CGLS-LC100), (b) livelihood zone data modified from USAID, famine early warning systems network (FEWS NET).

uncertainties related to data and algorithms. Our ALS data cover a wide range of vegetation types, large elevation gradient, and relatively large area, but it does not include the complete topographic and climatic gradient in the region. This can limit the predictive performance of the model in extreme elevations (i.e., highest and lowest areas outside ALS elevation ranges) and ecosystems not covered by the data. Availability of additional ALS data would increase the number of representative samples and improve WC prediction performance in the region. Nonetheless, over ALS site, our WC prediction and three global products (MODIS continuous vegetation fields, Landsat continuous vegetation fields from Global Forest Cover Change Tree Cover (GFCC), and Project for On-Board Autonomy – Vegetation (PROBA-V) tree cover) were compared against ALS woody cover (Fig. 13a–d). The comparison showed better performance of our model ($r^2 = 0.77$ and RMSE =12.9%) than global products, indicating improved capability of our approach in estimating WC. Strong underestimation of tree cover was displayed for MOD44B and GFCC Landsat continuous vegetation fields products in comparison to our prediction and PROBA-V tree cover. Yet for robust comparison in the region, reference ALS data that cover wider topographic and climatic gradient is needed in the future.

The non-parametric machine learning regression algorithms are important for extrapolating fractional WC. However, as regression uses central or mean values, extreme WC fraction values (i.e., 0% and 100%) are difficult to predict using regression model (Masiliūnas et al., 2021; Fig. 13). To minimize this problem and increase model performance, we trained the model using random samples stratified by ALS fractional WC bins. Despite its better performance, our result still underestimates higher values (>80%) when aggregated at 250 m resolution (Fig. 13c). In this regards, further studies towards improved machine learning algorithms are important in the future.

The fractional WCC result considers only areas that have underwent statistically significant ($P < 0.05$) changes. There could be degraded areas not included for statistical reason, yet important from management purpose. The choice of appropriate statistical threshold for detecting WC changes will be something to explore in the future.

The contribution of cropland expansion on WCC was estimated using 2019 crop fraction data at 100 m resolution from CGLS due to lack of temporally consistent, continuous fields of cropland fraction time series at 30 m resolution for the years 2001 to 2019. However, for better estimation of the contribution of cropland expansion on WCC, availability and use of such data is important in the future as changes occur at smaller scale in heterogeneous landscape such as in our study area.

Detailed quantitative analysis on the relative contribution of natural and anthropogenic factors to WCC is an important topic for future studies. Whether these factors have linear or non-linear relation with WCC, presence of complex interactions among predictor variables, and presence of causal links and strength of relationships need to be explored further considering additional factors, such as enhanced atmospheric CO2 concentration and change in herbivore densities.

## 6. Conclusion

In this study, we analyzed fractional WCCs in East Africa during 2001–2019. New WC loss hotspots and degradation corridor, which were not captured in global products, were identified near protected areas and in agricultural lands located close to pastoral and agropastoral boundaries.

The study revealed that WC dynamics are dominated by abrupt

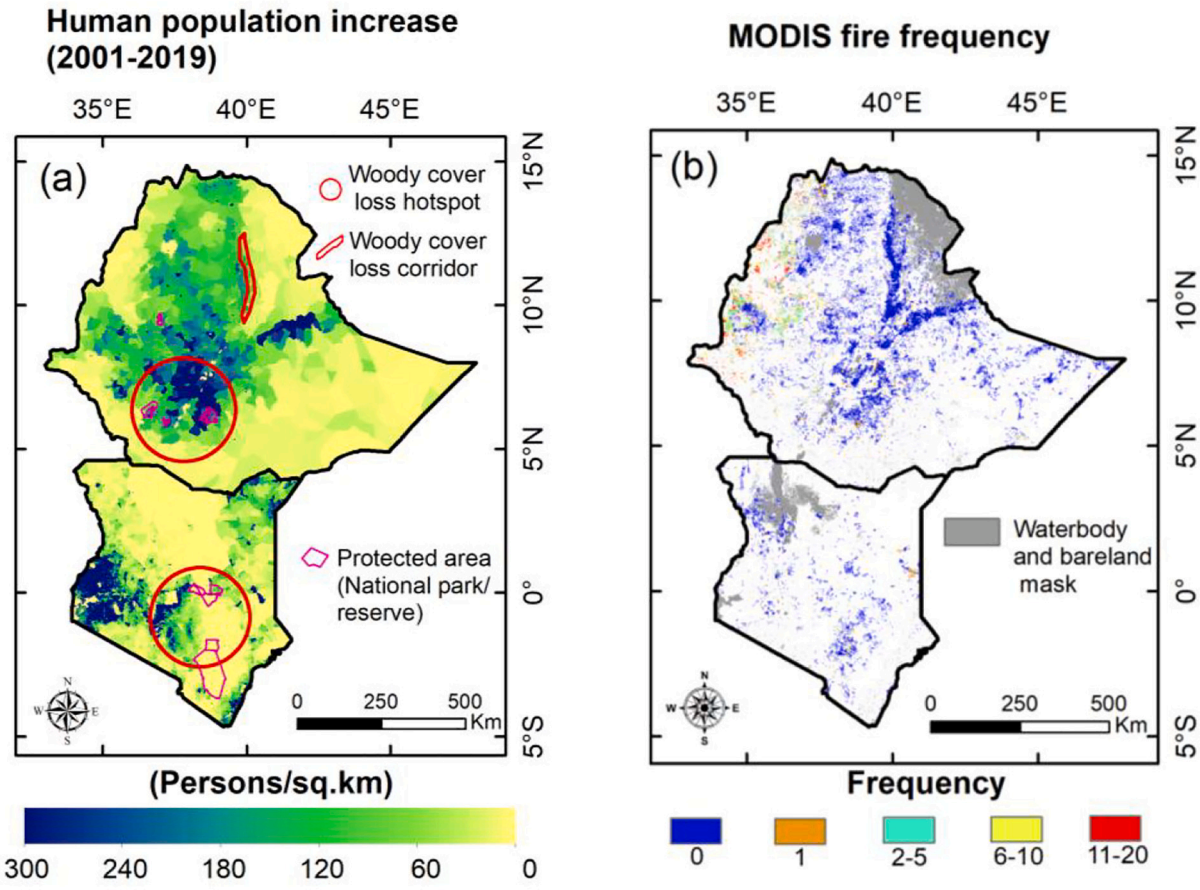


**Fig. 12.** Panel showing (a) trend of human population density, and (b) fire frequency during 2001–2019. Fire frequency plot is masked by fractional woody cover change pixels.

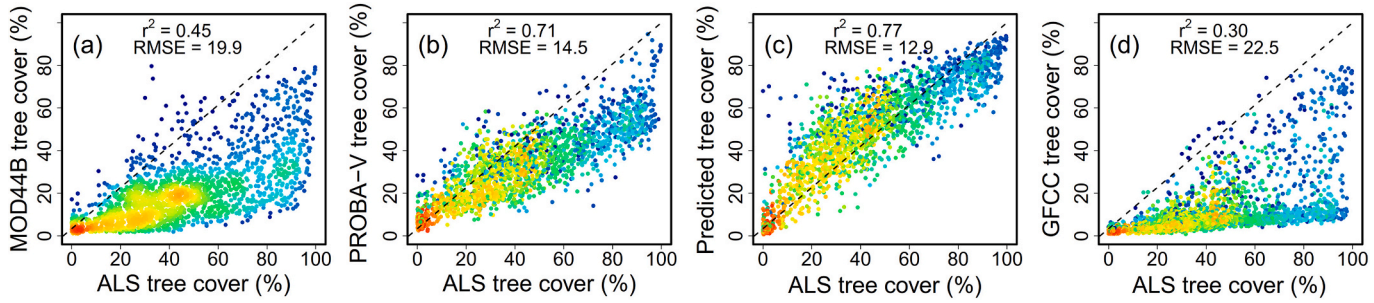


**Fig. 13.** Comparison of reference airborne laser scanning (ALS) tree cover estimate against (a) MODIS continuous vegetation fields fractional tree cover, (b) PROBA-V (Project for On-Board Autonomy - Vegetation) tree cover, (c) predicted tree cover, and (d) Landsat continuous vegetation fields from Global Forest Cover Change Tree Cover (GFCCTC30m v3). Comparison made for the year 2015 and at 250 m resolution.

changes. Woody cover losses strongly outweigh gains in both abrupt and gradual changes. Consequently, changes in fractional WC were dominated by net loss across all ecosystems. Comparatively, Acacia-Commiphora ecosystem experienced the highest WC loss and is the most threatened ecosystem in the region. While cropland expansion played major role (57%) in inducing WC loss, fuelwood extraction could have important impact as it mainly uses *Acacia-Commiphora* trees. Promoted by high population growth, cropland expansion and fuelwood extraction are likely to pose strong pressure on woody vegetation cover in the coming decades if not managed properly.

Applying satellite observation timeseries (MODIS and Landsat) with machine learning and non-parametric breakpoint detection algorithm helps to improve monitoring of woody cover change in the region. Overall, our results highlight, on one hand, the importance of improved approach for detecting and measuring the impact of human activities and livelihoods on woody vegetation cover and on the other hand, the necessity of protecting woody vegetation and evaluating existing land use practices in and around protected areas for assuring sustainable ecosystem service provision in the region.

## Credit author statement

Temesgen Alemayehu Abera, conception, methodology design, analysis, and writing; Janne Heiskanen, conception, methodology design, writing, and commenting; Eduardo Eiji Maeda, methodology design and commenting; Binyam Tesfaw Hailu, commenting; Petri K. E.

Pellikka, commenting and supervision.

## Declaration of Competing Interest

The authors declare that they have no conflict of interest.

## Acknowledgements

We would like to acknowledge ESSA (Earth observation and environmental sensing for climate-smart sustainable agropastoral ecosystem transformation in East Africa) project funded by European Union DG International Partnerships under DeSIRA (Development of Smart Innovation through Research in Agriculture) programme (FOOD/2020/418-132). Eduardo Maeda acknowledges funding from Academy of Finland (decision numbers 318252 and 319905), and Petri Pellikka acknowledges Academy of Finland funding for SMARTLAND (decision number 318645). We thank Martha Munyao, researcher at Kenya Wildlife Service and University of Helsinki, for her constructive discussions and comments. We appreciate anonymous reviewers for their valuable comments on the manuscript.

## Appendix A. Supplementary data

Supplementary data to this article can be found online at https://doi.org/10.1016/j.rse.2022.112897.

## References

Abera, T.A., Heiskanen, J., Pellikka, P.K.E., Maeda, E.E., 2018. Rainfall–vegetation interaction regulates temperature anomalies during extreme dry events in the horn of Africa. Glob. Planet. Chang. 167 (March), 35–45. https://doi.org/10.1016/j.gloplacha.2018.05.002.

Abera, T.A., Heiskanen, J., Pellikka, P.K.E., Adhikari, H., Maeda, E.E., 2020a. Climatic impacts of bushland to cropland conversion in eastern Africa. Sci. Total Environ. 717, 137255 https://doi.org/10.1016/j.scitotenv.2020.137255.

Abera, T.A., Heiskanen, J., Pellikka, P.K.E., Maeda, E.E., 2020b. Impact of rainfall extremes on energy exchange and surface temperature anomalies across biomes in the horn of Africa. Agric. For. Meteorol. 280, 107779 https://doi.org/10.1016/j.agrformet.2019.10777.

Adhikari, Hari, Heiskanen, J., Maeda, E.E., Pellikka, P.K.E., 2016. The effect of topographic normalization on fractional tree cover mapping in tropical mountains: an assessment based on seasonal Landsat time series. Int. J. Appl. Earth Obs. Geoinf. 52 (2016), 20–31. https://doi.org/10.1016/j.jag.2016.05.008.

Amara, E., Adhikari, H., Heiskanen, J., Siljander, M., Munyao, M., Omondi, P., Pellikka, P., 2020. Aboveground biomass distribution in a multi-use Savannah landscape in southeastern Kenya: impact of land use and fences. Land 9 (10), 381. https://doi.org/10.3390/land9100381.

Axelsson, C.R., Hanan, N.P., 2018. Rates of woody encroachment in African savannas reflect water constraints and fire disturbance. J. Biogeogr. 45, 1209–1218. https://doi.org/10.1111/jbi.13221.

Baig, M.H.A., Zhang, L., Shuai, T., Tong, Q., 2014. Derivation of a tasselled cap transformation based on Landsat 8 at-satellite reflectance. Remote Sens. Lett. 5 (5), 423–431. https://doi.org/10.1080/2150704X.2014.915434.

Bekele, M., Zewdie, S., Boissiere, M., Atmadja, S., 2018. REDD+ MRV implementation in Ethiopia: Review of the context, framework and progress. In: Occasional Paper 192. CIFOR, Bogor, Indonesia.

Bernard, F., Minang, P.A., Adkins, B., Freund, J.T., 2014. REDD+ projects and national-level readiness processes: a case study from Kenya. Clim. Pol. 14 (6), 788–800. https://doi.org/10.1080/14693062.2014.905440.

Borges, J., Higginbottom, T.P., Symeonakis, E., Jones, M., 2020. Sentinel-1 and Sentinel-2 data for Savannah land cover mapping: Optimising the combination of sensors and seasons. Remote Sens. 12, no. 23, 3862. https://doi.org/10.3390/rs12233862.

Bouvet, A., Mermoz, S., Le Toan, T., Villard, L., Mathieu, R., Naidoo, L., Asner, G.P., 2018. An above-ground biomass map of African savannahs and woodlands at 25 m resolution derived from ALOS PALSAR. Remote Sens. Environ. 206 (November 2017), 156–173. https://doi.org/10.1016/j.rse.2017.12.030.

Brandt, M., Rasmussen, K., Peñuelas, J., et al., 2017. Human population growth offsets climate-driven increase in woody vegetation in sub-Saharan Africa. Nat Ecol Evol 1, 0081. https://doi.org/10.1038/s41559-017-0081.

Brink, A.B., Bodart, C., Brodsky, L., Defourney, P., Ernst, C., Donney, F., Tuckova, K., 2014. Anthropogenic pressure in East Africa-monitoring 20 years of land cover changes by means of medium resolution satellite data. Int. J. Appl. Earth Obs. Geoinf. 28 (1), 60–69. https://doi.org/10.1016/j.jag.2013.11.006.

Brown, L., Chen, J.M., Leblanc, S.G., Cihlar, J., 2000. A shortwave infrared modification to the simple ratio for LAI retrieval in boreal forests: an image and model analysis. Remote Sens. Environ. 41 (1), 16–25. https://doi.org/10.1016/S0034-4257(99)00035-8.

Buchhorn, M., Lesiv, M., Tsendbazar, N.-E., Herold, M., Bertels, L., Smets, B., 2020. Copernicus global land cover layers—collection 2. Remote Sens. 12, 1044. https://doi.org/10.3390/rs12061044.

Burrell, A.L., Evans, J.P., Liu, Yi, 2017. Detecting dryland degradation using time series segmentation and residual trend analysis (TSS-RESTREND). Remote Sens. Environ. 197 (2017), 43–57. https://doi.org/10.1016/j.rse.2017.05.018.

Chidumayo, E.N., Gumbo, D.J., 2013. The environmental impacts of charcoal production in tropical ecosystems of the world: a synthesis. Energy Sust. Develop. 17 (2), 86–94. https://doi.org/10.1016/j.esd.2012.07.004.

Choat, B., Jansen, S., Brodribb, T., et al., 2012. Global convergence in the vulnerability of forests to drought. Nature 491, 752–755. https://doi.org/10.1038/nature11688.

De Jong, R., Verbesselt, J., Zeileis, A., Schaepman, M.E., 2013. Shifts in global vegetation activity trends (2013). Remote Sens. 5 (3), 1117–1133. https://doi.org/10.3390/rs5031117.

DeVries, B., Pratihast, A.K., Verbesselt, J., Kooistra, L., Herold, M., 2016. Characterizing Forest change using community-based monitoring data and Landsat time series. PLoS One 11 (3), e0147121. https://doi.org/10.1371/journal.pone.0147121.

DiMiceli, C., Carroll, M., Sohlberg, R., Kim, D., Kelly, M., Townshend, J., 2015. MOD44B MODIS/Terra Vegetation Continuous Fields Yearly L3 Global 250m SIN Grid V006 [Data set]. NASA EOSDIS Land Processes DAAC. Accessed 2021-03-24 from. https://doi.org/10.5067/MODIS/MOD44B.006.

Dinerstein, D., Olson, A., Joshi, C., Vynne, N.D., Burgess, E., Wikramanayake, ..., Saleem, M., 2017. An ecoregion-based approach to protecting half the terrestrial realm. BioScience 67 (6), 534–545. https://doi.org/10.1093/biosci/bix014.

FAO, 2020. Global Forest Resources Assessment Report, Ethiopia. Rome, 2020. http://www.fao.org/3/ca9991en/ca9991en.pdf.

Fenner, M., 1982. Aspects of the ecology of Acacia-Commiphora woodland near kibwezi, Kenya. J. East Africa Nat. History Soc. Nat. Museum 175, 1–11. http://ir-library.ku.ac.ke/handle/123456789/5818.

Forzieri, G., Miralles, D.G., Ciais, P., et al., 2020. Increased control of vegetation on global terrestrial energy fluxes. Nat. Clim. Chang. 10, 356–362. https://doi.org/10.1038/s41558-020-0717-0.

Franch, B., Vermote, E.F., Sobrino, J.A., Fédèle, E., 2013. Analysis of directional effects on atmospheric correction. Remote Sens. Environ. 128, 276–288. https://doi.org/10.1016/j.rse.2012.10.018.

Friis, Ib, Demissew, S., van Breugel, P., 2010. Atlas of the potential vegetation of Ethiopia. In: The Royal Danish Academy of Science and Letters. https://www.royalacademy.dk/Publications/Low/3607_Friis,%20Ib,%20Demissew,%20Sebsebe%20and%20van%20Breugel,%20Paulo.pdf.

Ghebreab, W., Yohannes, E., Giorgis, L.W., 1992. The Lega Dembi gold mine: an example of shear zone-hosted mineralization in the Adola greenstone belt, southern Ethiopia. J. African Earth Sci. (and the MiddleEast) 15 (3–4), 489–500. https://doi.org/10.1016/0899-5362(92)90030-G.

Giglio, L., Justice, C., Boschetti, L., Roy, D., 2015. MCD64A1 MODIS/Terra+aqua burned area monthly L3 global 500m SIN grid V006. NASA EOSDIS land processes DAAC. Accessed 2021-04-22 from. https://doi.org/10.5067/MODIS/MCD64A1.006.

Githiomi, J.M., Oduor, N., 2012. Strategies for sustainable wood fuel production in Kenya. Int J Appl Technol 2 (10), 21–25. https://citeseerx.ist.psu.edu/viewdoc/download?doi=10.1.1.1043.374&rep=rep1&type=pdf.

Gorelick, N., Hancher, M., Dixon, M., Ilyushchenko, S., Thau, D., Moore, R., 2017. Google earth engine: planetary-scale geospatial analysis for everyone. Remote Sens. Environ. 202, 18–27. https://doi.org/10.1016/j.rse.2017.06.031.

Hansen, M., DeFries, R., Townshend, J.R., Sohlberg, R., Dimiceli, C., Carroll, M., 2002. Towards an Operational MODIS Continuous Field of Percent Tree Cover Algorithm.

Hansen, et al., 2013. High-resolution global maps of 21st-century Forest cover change. Science 342 (6160), 850–853. https://doi.org/10.1126/science.1244693.

Hothorn, T., Zeileis, A., 2008. Generalized maximally selected statistics. Biometrics 64 (4), 1263–1269. https://doi.org/10.1111/j.1541-0420.2008.00995.x.

Hothorn, T., Hornik, K., van de Wiel, M.A., Zeileis, A., 2008. Implementing a class of permutation tests: the coin package. J. Stat. Softw. 28 (8), 1–23. https://doi.org/10.18637/jss.v028.i08.

Huete, A.R., 1988. A soil-adjusted vegetation index (SAVI). Remote Sens. Environ. 25, 295–309. https://doi.org/10.1016/0034-4257(88)90106-X.

Huete, A., Didan, K., Miura, T., Rodriguez, E.P., Gao, X., Ferreira, L.G., 2002. Overview of the radiometric and biophysical performance of the MODIS vegetation indices. Remote Sens. Environ. 83 (1), 195–213. https://doi.org/10.1016/S0034-4257(02)00096-2.

Iiyama, M., Neufeldt, H., Dobie, P., Njenga, M., Ndegwa, G., Jamnadass, R., 2014. The potential of agroforestry in the provision of sustainable woodfuel in sub-Saharan Africa. Curr. Opin. Environ. Sustain. 6, 138–147. https://doi.org/10.1016/j.cosust.2013.12.003.

Kassa, H., Birhane, E., Bekele, M., Lemenih, M., Cronkleton, P., Putzel, L., Baral, H., 2017. Shared strengths and limitations of participatory forest management and area exclosure: two major state led landscape rehabilitation mechanisms in Ethiopia. Int. For. Rev. 19, 51–61.

Kendall, M.G., 1975. Rank Correlation Methods. Oxford University Press, New York, NY.

Kramer, P.J., Boyer, J.S., 1995. Water Relations of Plants and Soils. Academic press, Inc.

Li, W., Buitenwerf, R., Munk, M., Bøcher, P.K., Svenning, J.-C., 2020. Deep-learning based high-resolution mapping shows woody vegetation densification in greater Maasai Mara ecosystem. Remote Sens. Environ. 247, 111953 https://doi.org/10.1016/j.rse.2020.111953.

Lyapustin, A., Wang, Y., 2018. MCD19A3 MODIS/Terra+aqua BRDF model parameters 8-day L3 global 1km SIN grid V006 [data set]. NASA EOSDIS land processes DAAC. Accessed 2021-03-11 from. https://doi.org/10.5067/MODIS/MCD19A3.006.

Lyapustin, I., et al., 2012. Multi-angle implementation of atmospheric correction for MODIS (MAIAC): 3 Atmospheric correction. Remote Sens. Environ. 127, 385–393. https://doi.org/10.1016/j.rse.2012.09.002.
Mann, H.B., 1945. Nonparametric tests against trend. Econometrica 13, 245–259. https://doi.org/10.2307/1907187.
Masiliūnas, D., Tsendbazar, E.-R., Herold, M., Lesiv, M., Buchhorn, M., Verbesselt, Jan, 2021. Global land characterisation using land cover fractions at 100 m resolution. Remote Sens. Environ. 259, 112409 https://doi.org/10.1016/j.rse.2021.112409.
Mesfin, T., Menbere, I.P., 2020. Socio-economic and environmental values of Acacia-Commiphora (small-leaved deciduous) Forest in Ethiopia. J. Biol. Agricult. Healthcare 10 (23), 8–16. https://doi.org/10.7176/JBAH/10-23-02.
Mittermeier, R.A., Myers, N., Thomsen, J.B., Fonseca, G.A.B., Olivieri, S., 1998. Biodiversity hotspots and major tropical wilderness areas: approaches to setting conservation priorities. Conserv. Biol. 12, 516–520. https://doi.org/10.1046/j.1523-1739.1998.012003516.x.
Munyao, M., Siljander, M., Johansson, T., Makokha, G., Pellikka, P., 2020. Assessment of human–elephant conflicts in multifunctional landscapes of Taita Taveta County, Kenya. Global Ecol. Conservat. 24, e01382 https://doi.org/10.1016/j.gecco.2020.e01382.
Nicholson, S.E., 2017. Climate and climatic variability of rainfall over eastern Africa. Rev. Geophys. 55, 590–635. https://doi.org/10.1002/2016RG000544.
Pellikka, P.K.E., Heikinheimo, V., Hietanen, J., Schäfer, E., Siljander, M., Heiskanen, J., 2018. Impact of land cover change on aboveground carbon stocks in Afromontane landscape in Kenya. Appl. Geogr. 94, 178–189. https://doi.org/10.1016/j.apgeog.2018.03.017.
Pickering, J., Tyukavina, A., Khan, A., Potapov, P., Adusei, B., Hansen, M.C., Lima, A., 2021. Using multi-resolution satellite data to quantify land dynamics: applications of PlanetScope imagery for cropland and tree-cover loss area estimation. Remote Sens. 13, 2191. https://doi.org/10.3390/rs13112191.
Potapov, P., Hansen, M.C., Stehman, S.V., Loveland, T.R., Pittman, K., 2008. Combining MODIS and Landsat imagery to estimate and map boreal forest cover loss. Remote Sens. Environ. 112 (9), 3708–3719. https://doi.org/10.1016/j.rse.2008.05.006.
Potapov, P., Tyukavina, A., Turubanova, S., Talero, Y., Hernandez-Serna, A., Hansen, M. C., Nguyen, Q.H., 2019. Annual continuous fields of woody vegetation structure in the lower Mekong region from 2000-2017 Landsat time-series. Remote Sens. Environ. 232, 111278 https://doi.org/10.1016/j.rse.2019.111278.
Rippke, U., Ramirez-Villegas, J., Jarvis, A., et al., 2016. Timescales of transformational climate change adaptation in sub-Saharan African agriculture. Nat. Clim. Chang. 6, 605–609. https://doi.org/10.1038/nclimate2947.
Roy, D.P., Kovalskyy, V., Zhang, H.K., Vermote, E.F., Yan, L., Kumar, S.S., Egorov, A., 2016. Characterization of Landsat-7 to Landsat-8 reflective wavelength and normalized difference vegetation index continuity. Remote Sens. Environ. 185, 57–70. https://doi.org/10.1016/j.rse.2015.12.024.
Schaaf, C., Wang, Z., 2015. MCD43A4 MODIS/Terra+Aqua BRDF/Albedo Nadir BRDF Adjusted Ref Daily L3 Global - 500m V006. NASA EOSDIS Land Processes DAAC. Accessed 2021-01-10 from. https://doi.org/10.5067/MODIS/MCD43A4.006.
Schultz, M., Verbesselt, J., Avitabile, V., Souza, C., Herold, M., 2016. Error sources in deforestation detection using BFAST monitor on Landsat time series across three tropical sites. IEEE J. Selected Top. Appl. Earth Observat. Remote Sens. 9 (8), 3667–3679. https://doi.org/10.1109/JSTARS.2015.2477473.
SEDAC (NASA Socioeconomic Data and Applications Center), 2021. Center for International Earth Science Information Network - CIESIN - Columbia University Gridded Population of the World, Version 4 (GPWv4): Population Density, Revision 11. accessed April 2021. https://doi.org/10.7927/H49C6VHW.
Sexton, et al., 2013. Global, 30-m resolution continuous fields of tree cover: Landsat-based rescaling of MODIS vegetation continuous fields with lidar-based estimates of error. Int. J. Dig. Earth 6 (5), 427–448. https://doi.org/10.1080/17538947.2013.786146.
Sola, P., Cerutti, P.O., Zhou, W., et al., 2017. The environmental, socioeconomic, and health impacts of woodfuel value chains in sub-Saharan Africa: a systematic map. Environ Evid 6, 4. https://doi.org/10.1186/s13750-017-0082-2.
Stévart, T., et al., 2019. A third of the tropical African flora is potentially threatened with extinction. Science. Advances 5 (11), eaax9444. https://doi.org/10.1126/sciadv.aax9444.
Sulla-Menashe, D., Friedl, M.A., 2018. User Guide to Collection 6 MODIS Land Cover (MCD12Q1 and MCD12C1) Product. https://lpdaac.usgs.gov/documents/101/MCD12_User_Guide_V6.pdf.
UNEP, 2016. The contribution of forests to national income in Ethiopia and linkages with REDD+. In: United Nations environment Programme: Nairobi. UN-REDD Programme, 1-65. https://wedocs.unep.org/bitstream/handle/20.500.11822/23024/forests_income_ethiopia.pdf?sequence=1&isAllowed=y (accessed on April 2021).
van Breugel, P., Friis, I., Demissew, S., et al., 2016. Current and future fire regimes and their influence on natural vegetation in Ethiopia. Ecosystems 19, 369–386. https://doi.org/10.1007/s10021-015-9938-x.
Venter, Z.S., Cramer, M.D., Hawkins, H.J., 2018. Drivers of woody plant encroachment over Africa. Nat. Commun. 9, 2272. https://doi.org/10.1038/s41467-018-04616-8.
Verbesselt, J., Hyndman, R., Newnham, G., Culvenor, D., 2010. Detecting trend and seasonal changes in satellite image time series. Remote Sens. Environ. 114 (1), 106–115. https://doi.org/10.1016/j.rse.2009.08.014.
Vuorinen, P., Tesemma, M., Laxen, J., Hamalainen, J., Pieper, G., Hailu, B., Roba, B., Bekele, M., 2016. Study of Causes of Deforestation and Forest Degradation in Ethiopia and the Identification and Prioritization of Strategic Options to Address those. Oy Arbonaut Ltd, FM-International OY FINNMAP and Baseline Surveying Engineering Consultant. https://ethiopiareddplus.gov.et/wp-content/uploads/2017/06/National-study-on-drivers-of-deforestation-and-forest-degradation-ethiopia-final.pdf.
White, F., 1983. The vegetation of Africa: a descriptive memoir to accompany the UNESCO/AETFAT/UNSO vegetation map of Africa. Nat. Resour. Res. 20 (1983) https://doi.org/10.2307/2260340.
Wilcox, R., 1998. A note on the Theil-Sen regression estimator when the regressor is random and the error term is heteroscedastic. Biometrical J. 40 (3), 261–268. https://doi.org/10.1002/(SICI)1521-4036(199807)40:3<261::AID-BIMJ261>3.0.CO;2-V.
Williams, C.A., Hanan, N.P., Neff, J.C., et al., 2007. Africa and the global carbon cycle. Carbon Balance Manag. 2, 3. https://doi.org/10.1186/1750-0680-2-3.
Williams, A.P., et al., 2012. Drought stress and tree mortality. Nat. Clim. Chang. 3 (2012), 292–297. https://doi.org/10.1038/nclimate1693.
Zeileis, A., Hothorn, T., 2013. (2013). A toolbox of permutation tests for structural change. Stat. Pap. 54, 931–954. https://doi.org/10.1007/s00362-013-0503-4.
Zhang, W., Brandt, M., Wang, Q., Prishchepov, A.V., Tucker, C.J., Li, Y., Lyu, H., Fensholt, R., 2019. From woody cover to woody canopies: how Sentinel-1 and Sentinel-2 data advance the mapping of woody plants in savannas. Remote Sens. Environ. 234 (2019), 111465 https://doi.org/10.1016/j.rse.2019.111465.